Neurons of the inferior olive respond to broad classes of sensory input while subject to homeostatic control

Homeostatic complex spike firing

Chiheng Ju[1,3], Laurens W.J. Bosman[1,3*], Tycho M. Hoogland[1,2,3*], Arthiha Velauthapillai[1], Pavithra Murugesan[1], Pascal Warnaar[1], Mario Negrello[1] and Chris I. De Zeeuw[1,2]

[1] Department of Neuroscience, Erasmus MC, 3015 GD Rotterdam, The Netherlands

[2] Netherlands Institute for Neuroscience, Royal Netherlands Academy of Arts and Sciences, 1105 BE Amsterdam, The Netherlands

[3] These authors contributed equally

* Correspondence to Dr. Laurens Bosman, PO Box 2040, 3000 CA Rotterdam, The Netherlands, l.bosman@erasmusmc.nl; or to Dr. Tycho Hoogland, PO Box 2040, 3000 CA Rotterdam, The Netherlands, t.hoogland@erasmusmc.nl

No. of figures:	9 (+ 4 Tables)
No. of words for Abstract:	231
No. of words for Introduction:	650
No. of words for Discussion:	1498

The authors declare no competing financial interests.

Acknowledgements

The authors wish to thank A.C.H.G. IJpelaar for technical assistance and Dr. M. Schonewille for help with recording ocular movements during stimulation. Financial support was provided by the Netherlands Organization for Scientific Research (NWO-ALW; C.I.D.Z.), the Dutch Organization for Medical Sciences (ZonMW; C.I.D.Z.), Life Sciences (C.I.D.Z.), ERC-adv and ERC-POC (C.I.D.Z.) and the China Scholarship Council (No. 2010623033; C.J.).

Abstract

Purkinje cells in the cerebellar cortex fire complex spikes in response to sensory stimulation. These complex spikes are triggered by activity of climbing fibers originating in neurons of the inferior olive. The neurons of the inferior olive are electrically coupled. Strong sensory input has been shown to preferentially recruit coherent climbing fiber activity within one or more specific parasagittal microzones of Purkinje cells, but it is unclear to what extent different types of sensory inputs can drive complex spikes within the same Purkinje cells and how the strength as well as the history of these inputs influence climbing fiber activity. Here, we characterized complex spike responses in crus 1 and crus 2 to various types of sensory stimulation in awake male mice using two-photon calcium imaging. We find that stimulations of different sensory modalities and at different locations have a weak, but consistent, tendency to converge on individual Purkinje cells. The Purkinje cells encoding the same stimulus show increased coherence in their firing patterns and tend to lie close together. Moreover, the complex spike response probability increases when the inter-trial intervals decrease, whereas it depends only weakly on the strength of the sensory stimulus. Our data point towards a mechanism in the olivo-cerebellar system that regulates complex spike firing during mono- or multisensory stimulation around a relatively low set-point, highlighting an integrative coding scheme of complex spike firing under homeostatic control.

Significance statement

Whether sleeping or waking, climbing fibers derived from the inferior olive trigger complex spikes in cerebellar Purkinje cells at a rate of roughly once a second. Complex spikes can be evoked by sensory stimulation and affect motor output. Here, we show that sensory evoked complex spikes come at the expense of spontaneously occurring complex spikes, suggesting a homeostatic mechanism. Subject to this homeostatic mechanism, individual Purkinje cells can respond with complex spikes to a wide variety of sensory stimulations varying from subtle and specific forms up to combinations of different origins. Purkinje cells that share the same sensitivity for a particular input pattern tend to fire coherently and are located in each other's vicinity.

Introduction

Sensorimotor integration is a brain-wide phenomenon with a crucial olivo-cerebellar contribution. The climbing fibers that originate in the inferior olive and cause complex spike firing in cerebellar Purkinje cells (PCs) encode both unexpected and expected sensory events and affect initiation, execution and adaptation of movements (Albus, 1971; Welsh et al., 1995; Kitazawa et al., 1998; Gibson et al., 2004; Bosman et al., 2010; Yang and Lisberger, 2014; Ten Brinke et al., 2015; Streng et al., 2017; Brown and Raman, 2018; Herzfeld et al., 2018; Romano et al., 2018). The complex spike frequency is typically around 1 Hz and not substantially affected by the behavioral state (Bloedel and Ebner, 1984; Mukamel et al., 2009; Bosman et al., 2010; Zhou et al., 2014). The paradox between persistent complex spike firing and the behavioral relevance of individual complex spikes is still largely unresolved. As awareness grows that cerebellar contributions exceed sensorimotor control (Schmahmann, 2004; Rahmati et al., 2014; Peter et al., 2016), understanding the function of the reciprocal and exceptionally strong cerebello-cerebral cortical pathways (Keser et al., 2015; Schäfer and Hoebeek, 2018) becomes increasingly relevant. A clearer picture of complex spike response dynamics and the related anatomical organization of sensory input to PCs is therefore required.

The anatomical organization of sensory input to the cerebellum underlies conflicting views. The strong divergence and convergence of afferents and efferents (Harvey and Napper, 1991; Sugihara et al., 2001; Person and Raman, 2011) suggest an integrative role of PCs, processing ascending and descending inputs, while the organization of somatosensory input into a fractured somatotopy suggests the existence of specialized areas within the cerebellar cortex (Miles and Wiesendanger, 1975; Joseph et al., 1978; Shambes et al., 1978; Rushmer et al., 1980; Robertson et al., 1982; Castelfranco et al., 1994; Apps and Hawkes, 2009). Such

spatial heterogeneity agrees with the recently discovered link between anatomical modules, identified by their zebrin expression pattern, and variability in PC activity and plasticity (Xiao et al., 2014; Zhou et al., 2014; Cerminara et al., 2015; De Zeeuw and Ten Brinke, 2015; Tsutsumi et al., 2015).

Electrical stimulation of major nerves of cat limbs have demonstrated adherence of climbing fiber projections to parasagittal zones (Oscarsson, 1969; Groenewegen et al., 1979), which can be further differentiated into smaller microzones based upon their response pattern to tactile stimulation of a particular spot on the body (Ekerot et al., 1991; Apps and Garwicz, 2005; Ozden et al., 2009; De Zeeuw et al., 2011). Nearby PCs receive climbing fiber input predominantly from adjacent inferior olivary neurons characterized by dense gap junctional coupling promoting synchronization of their output (Sotelo et al., 1974; De Zeeuw et al., 1995; Devor and Yarom, 2002; Van Der Giessen et al., 2008). The existence of sensory maps at sub-microzonal levels has not yet been investigated. Moreover, it is unclear whether these maps depend on the recent stimulation history.

Using minimal stimuli of distinct sensory modalities with different durations, we asked whether a more detailed response pattern could be created and whether previous activity mattered. Using two-photon Ca^{2+} imaging of crus 1 and 2 in awake mice, allowing reliable detection of complex spikes in adjacent PCs (Mukamel et al., 2009; De Gruijl et al., 2014; Hoogland et al., 2015), we contrasted strong sensory stimulation, using whisker air puffs, with more subtle stimuli comprising touches on four facial areas as well as sound and light stimuli. We found that PCs respond to multiple inputs, with PCs encoding the same stimulus type having a tendency to come together in groups more fine-grained than microzones. Analysis of complex spike coherence confirmed the importance of population coding, with sensory-evoked complex spike coming at the expense of spontaneously generated complex spikes. Altogether, our data show that weak and local sensory input recruit

mosaic ensembles of PCs, employing population coding in a spatially more dynamic way than would be predicted from hard-wired microzones, and underlie strong homeostasis in the temporal domain.

Materials and Methods

Animals and surgery

All experimental procedures involving animals were in agreement with Dutch and European legislation and guidelines and approved in advance by an independent ethical committee (DEC Consult, Soest, The Netherlands) as required by Dutch law. Mice were group housed until the day of the experiment and kept under a regime with 12 h light and 12 h dark with food and water available *ad libitum*. The mice had not been used for other experiments prior to the ones described here.

For the experiments performed in awake mice, we recorded from in total 66 areas located in cerebellar lobules crus 1 and crus 2 of 29 male C57Bl/6J mice of 4-12 weeks of age (Charles Rivers, Leiden, The Netherlands). Prior to surgery, mice were anesthetized using isoflurane (initial concentration: 4% V/V in O_2, maintenance concentration: ca. 2% V/V) and received Carprofen (Rimadyl, 5 mg/ml subcutaneously) to reduce post-surgical pain. To prevent dehydration, mice received 1 ml of saline s.c. injection before the surgeries commenced. Eyes were protected using eye ointment (Duratears, Alcon, Fort Worth, TX, USA). Body temperature was maintained using a heating pad in combination with a rectal thermometer. During surgery, we attached a metal head plate to the skull with dental cement (Superbond C&B, Sun Medical Co., Moriyama City, Japan) and made a craniotomy with a diameter of approximately 2 mm centered on the medial part of crus 1 ipsilateral to the side of somatosensory stimulation. The dura mater was preserved and the surface of the cerebellar cortex was cleaned with extracellular solution composed of (in mM) 150 NaCl, 2.5 KCl, 2 $CaCl_2$, 1 $MgCl_2$ and 10 HEPES (pH 7.4, adjusted with NaOH). After the surgery, the mice were allowed to recover from anesthesia for at least 30 minutes. Subsequently, the mice were head-fixed in the recording setup and they received a bolus-loading of the Ca^{2+} indicator Cal-

520 (0.2 mM; AAT Bioquest, Sunnyvale, CA) (Tada et al., 2014). The dye was first dissolved with 10% w/V Pluronic F-127 in DMSO (Invitrogen, Thermo Fisher Scientific, Waltham, MA, USA) and then diluted 20 times in the extracellular solution. The dye solution was pressure injected into the molecular layer (50–80 μm below the surface) at 0.35 bar for 5 min. Finally, the brain surface was covered with 2% agarose dissolved in saline (0.9% NaCl) in order to reduce motion artifacts and prevent dehydration.

For the experiments on single-whisker stimulation we made recordings under anesthesia on 17 male C57BL/6J mice of 4-12 weeks of age. The procedure was largely the same as described above, but instead of isoflurane we used ketamine/xylazine (i.p. injection via butterfly needle, initial dose: 100 mg/kg and 10 mg/kg, respectively; maintenance dose: approximately 60 mg/kg/h and 3 mg/kg/h, respectively). The mice remained under anesthesia until the end of the recording. A subset of these experiments was performed with 0.2 mM Oregon Green BAPTA-1 AM dye (Invitrogen) as this dye has been more widely used than Cal-520 (e.g., Stosiek et al., 2003; Ozden et al., 2009; Schultz et al., 2009; Hoogland et al., 2015). Oregon Green BAPTA-1 AM was dissolved and applied in the same way as Cal-520. We found that Cal-520 had a superior signal-to-noise ratio under our experimental conditions. As a consequence, the observed event rate was lower in the experiments using OGB-1 (OGB-1: 0.45 ± 0.26 Hz; n = 172 cells; Cal-520: 0.72 ± 0.40 Hz; n = 43 cells; median ± IQR; U = 1719.0, p < 0.001, Mann-Whitney test). The observed frequency range using Cal-520 was comparable to that found using *in vivo* single-unit recordings under ketamine/xylazine anesthesia: 0.6 ± 0.1 Hz (Bosman et al., 2010). Despite an underestimation of the complex spike rate using OGB-1, we found that the ratios of PCs that responded to single whisker stimulation were similar for both dyes (OGB-1: 89 out of 373 cells (24%); Cal-520: 35 out of 152 cells (23%); p = 0.910; Fisher's exact test). For this reason, we combined the data from both dyes. For the analysis presented in Figure 5, we included only those cells that could be

recorded during all stimulus conditions. All experiments using awake data were obtained with Cal-520.

In vivo *two-photon Ca^{2+} imaging*

Starting at least 30 min after dye injection, *in vivo* two-photon Ca^{2+} imaging was performed of the molecular layer using a setup consisting of a Ti:Sapphire laser (Chameleon Ultra, Coherent, Santa Clara, CA, USA), a TriM Scope II system (LaVisionBioTec, Bielefeld, Germany) mounted on a BX51 microscope with a 20x 1.0 NA water immersion objective (Olympus, Tokyo, Japan) and GaAsP photomultiplier detectors (Hamamatsu, Iwata City, Japan). A typical recording sampled a field of view of 40 x 200 µm with a frame rate of approximately 25 Hz.

Sensory stimulation

Cutaneous stimuli were delivered to four defined regions on the left side of the face, ipsilateral to side of the craniotomy. These regions were the whisker pad, the cheek posterior to the whisker pad, the upper lip and the lower lip. Stimuli were applied using a Von Frey filament (Touch Test Sensory Evaluator 2.83, Stoelting Co., IL, USA) attached to a piezo linear drive (M-663, Physik Instrumente, Karlsruhe, Germany). Prior to the set of experiments described here, we tested a series of 8 Von Frey filaments with a stiffness range from 0.02 g to 1.4 g in awake head-fixed mice to select the optimal force for these experiments. We selected the 0.07 g (0.686 mN) filament because this filament induced a mild reaction in the mouse, but no signs of a nociceptive response (cf. Chaplan et al. (1994)). The touch time was fixed at 100 ms. As a control, we moved the stimulator without touching the face ("sound only" condition). Visual stimuli were delivered as 10 ms pulses using a 460 nm LED (L-7104QBC-D, Kingbright, CA, USA). The stimulation frequency was fixed at 1 Hz and the

different stimuli were applied in a random order. Video-recordings of the eye, made under infrared illumination, revealed that the mice did not make eye movements in response to the LED flash, but they did show reflexive pupil constriction (*data not shown*).

Single whiskers were stimulated using a piezo linear drive (M-663, Physik Instrumente) while using a deflection of 6°. It took the stimulator approximately 30 ms to reach this position. In our analyses, we used the estimated moment of touch as the stimulus onset time. At the extreme position, the stimulator was paused for 150 ms before returning to the neutral position. The stimulator was designed to minimize contact with other whiskers. Each stimulation experiment consisted of five sessions in random order. During each block one of the ipsilateral whiskers B2, C1, C2, C3 and D2 was stimulated. Each session consisted of 150 stimuli at 2 or 3 Hz.

Image analysis

Image analysis was performed offline using custom made software as described and validated previously (Ozden et al., 2012; De Gruijl et al., 2014). In short, we performed independent component analysis to create a mask describing the locations of individual PC dendrites (Figure 2A). For each field of view, the mask was generated only once, so that the same PCs were analyzed for subsequent recordings of different stimulus conditions enabling paired comparisons. Experiments during which spatial drift occurred were discarded from subsequent analysis. The fluorescent values of all pixels in each region of interest were averaged per frame. A 8% rolling baseline was subtracted with a time window of 0.5 ms (Ozden et al. 2012) after which Ca^{2+} transient events were detected using template matching.

Experimental design and statistical analysis

In general, we first tested whether parameter values were distributed normally using one-sample Kolmogorov-Smirnov tests. If not, non-parametric tests were applied. When making multiple comparisons, we used ANOVA tests (or the non-parametric equivalents) or applied Bonferroni correction, as indicated in the relevant sections of the Results. For each experiment, stimulus conditions were given in a random sequence. Identification of PC dendrites and event extraction was performed in a fashion blind to the type of stimulus. For the experiments characterizing response characteristics of individual PCs (Figures 2-4) we compared the fraction of responsive PCs, the response latency and the response peak. After extracting the Ca^{2+} transient event times, peri-stimulus time histograms (PSTHs) were constructed using the inter-frame time (approx. 40 ms) as bin size. The stacked line plot shown in Figure 2E was created by first making a PSTH for the PC with the weakest peak response (red line), then adding the PSTH of the second-weakest PC, etc. The data were normalized such that the upper (blue) line represents the average value of all PCs. Significance of responses was tested using a bootstrap method: we shuffled the inter-spike intervals and created artificial PSTHs using the original stimulus times. This procedure was repeated 500 times and the resultant bootstrap-PSTHs were averaged. As threshold, we used the average + 2 sd. Response latency and amplitude of the response were only derived from PCs with a significant response. These parameters were compared using Kruskal-Wallis tests (Figure 3). To calculate whether two or more inputs converged on single PCs we also used a bootstrap method. First, we determined the fraction of responsive cells for each parameter and compared these to a randomly generated number between 0 and 1 as taken from a uniform distribution. If for each input the randomly generated numbers were lower than the measured fractions, we considered them as responsive to all stimuli. This procedure was repeated 10,000 times and the average and standard deviation were derived and used to calculate the *Z*

score of the experimental data. All bootstrap procedures were performed using custom-written code in LabVIEW (National Instruments, Austin, TX, USA). In order to reduce the experimental time under anesthesia, we used a higher stimulus frequency (2 or 3 Hz) for the single-whisker stimulation experiments. For these experiments, we calculated the baseline and variation based upon the 300 ms prior to the stimulus and took average + 3 sd as threshold for significance of a response.

The distributions of pairs of PCs, either both responsive to a given stimulus ("responsive pairs") or one cell being responsive and the other not ("heterogeneous pairs"), were tested using two-dimensional Kolmogorov-Smirnov tests performed in MatLab (MathWorks, Natick, MA, USA). Aggregate PSTHs (Figure 8) were constructed and evaluated as described before (Romano et al., 2018). Briefly, we calculated per individual frame the number of simultaneously occurring events and color coded these in a PSTH combining data from all dendrites in a field of view. Based upon the total number of complex spikes and dendrites per recording, we calculated the expected number of simultaneous complex spikes per individual frame based upon a Poisson distribution. The actual number of simultaneous complex spikes was compared to this calculated distribution and a p value was derived for each number based upon the Poisson distribution (using custom-written software in MatLab and LabVIEW).

Unless stated otherwise, statistical tests were performed using SPSS (IBM, Armonk, NY, USA) and data are represented in the text as average ± SEM.

Results

Climbing fibers relay tactile input

Little is known about the distribution and convergence of different types of climbing fiber-mediated sensory input at the level of individual, nearby PCs. Climbing fibers organize in parasagitally oriented bands, thereby creating parasagittal microzones of PCs. These microzones have been proposed to form "fundamental processing units" (Apps and Garwicz, 2005). On the other hand, cerebellar somatotopy is fractured, consisting of patches and not of stripes (Shambes et al., 1978; Robertson et al., 1982). Attempts to reconcile these views leave many questions open, in particular with regard to the organization at the cellular level (Apps and Hawkes, 2009). For this reason, we performed two-photon Ca^{2+} imaging of PCs in awake mice to record complex spikes induced by climbing fiber activity in response to various types of sensory stimulation. We started our study by using strong sensory stimulation, i.e. air puffs to the large facial whiskers. Sensory input from the facial whiskers reaches the inferior olive via a direct route from the trigeminal nuclei as well as indirectly via the cerebral cortex and the nuclei of the meso-diencephalic junction (Yatim et al., 1996; Bosman et al., 2011; Kubo et al., 2018) (Figure 1). In line with previous studies (Axelrad et al., 1977; Brown and Bower, 2002; Bosman et al., 2010; Brown and Raman, 2018; Romano et al., 2018), we show that crude air puff stimulation to the whiskers evokes complex spike responses in many PCs (e.g., in 19 out of 19 PCs illustrated in Figure 2). In total, we found that 102 out of the 118 cells analyzed (86%) were responsive to such a stimulus.

To address whether localized and more subtle stimuli can recruit smaller groups of PCs, maybe even subsets of microzones, we applied gentle tactile stimulation at four facial locations: the whisker pad, the cheek posterior to the whisker pad, the upper lip and the lower lip (Figure 3A) using a Von Frey filament (target force = 0.686 mN) attached to a piezo

actuator. The stimulus strength was carefully calibrated to be of the minimal strength required to evoke a response, but without inducing responses from neighboring skin areas or nociceptive responses (see Methods). As expected from gentle touches (Bosman et al., 2010), the response rates were low but discernible. Each of the stimulus types could recruit between 26 and 42% of all PCs measured (Figure 3B-D)

The touches were presented by a piezo-actuator that made a weak but audible sound. We also tested whether PCs responded to this sound in the absence of touch. This was the case, but only in 42 out of 154 PCs tested (27%). These stimuli were compared to a brief light flash - presented at 1 Hz - using a blue LED. This stimulus triggered pupil constriction, but no other form of ocular movement (*data not shown*). The visual stimulus resulted in 48 out of 141 PCs (34%) being responsive. Whisker pad, lower lip and visual stimulation activated more PCs than upper lip, cheek or auditory stimulation ($\chi^2(5) = 21.049$, $p < 0.001$, χ^2 test; Figure 3D, Table 1).

The strongest peak responses were elicited by cheek stimulation, closely followed by lower lip, visual and whisker pad stimulation. Touching the upper lip or applying the auditory stimulus resulted in lower response rates ($H(5) = 24.267$, $p < 0.001$, Kruskal-Wallis test; Figure 3E). This implies that the upper lip and the auditory stimulus engaged relatively few PCs in the recorded areas and caused weak responses, whereas whisker pad, lower lip and visual stimulation caused relatively strong responses in many cells. Cheek stimulation engaged few cells, but with relatively strong responses. All tactile stimuli and the auditory stimulation had comparable response latencies, but visual stimulation evoked complex spikes with a remarkably long latency time (126 ± 42 ms; median ± inter-quartile range; $p < 0.001$ compared to all other stimuli; post-hoc tests after Kruskal-Wallis test: $H(5) = 55.995$, $p < 0.001$; Figure 3F).

Next, we addressed whether PCs have a preference to respond to one or multiple types of stimulation. To test this, we assumed a random distribution of receptive fields over the PCs and calculated the expected overlaps using a bootstrap method. When considering only the tactile responses, the observed convergence of climbing fiber responses from different facial regions on single PCs was far from complete for each individual combination. The observed *Z* values were on the border of significance in the absence of correction for multiple comparisons (Tables 2 and 3). However, all combinations occurred more often than predicted and although the significance of each observation in isolation was not very strong, the fact that not a single combination occurred less often than expected allows the conclusion that there was a weak, but ubiquitous, tendency for tactile input from different facial regions to converge on individual PCs. Yet, a large heterogeneity was found in terms of the combinations of climbing fiber receptive fields between specific PCs (Figure 4A; Tables 2 and 3).

Since we used the sound of the mechanical stimulator as auditory stimulus, we expected a large overlap between auditory and tactile inputs. This was the case for the combinations of lower lip and sound and for cheek and sound, but not for the other two facial areas (Figure 4B; Table 2). We explain this by the low sound level of the auditory stimulus compared to the relatively noisy background of a two-photon setup. This is corroborated by the sparse and weak responses to auditory stimulation (cf. Figure 3D-E). Strong sounds can elicit complex spikes in many PCs as has been extensively studied in the context of eyeblink conditioning (Ten Brinke et al., 2015) and fall outside the scope of this project. We also found that – despite the difference in response latency – visual and tactile stimuli clearly converged on the same PCs (Figure 4C; Table 2). Overall we conclude that PCs have a weak but consistent tendency to combine climbing fiber input conveying different types of sensory input in a mosaic pattern.

Single whisker responses in PCs

Using single-unit electrophysiological recordings we have previously shown that the stimulation of a single whisker is sufficient to evoke complex spike responses (Bosman et al., 2010). We reasoned that single whiskers would therefore qualify as minimal receptive fields that could evoke responses within a microzone (cf. Apps and Garwicz (2005)). In order to look at responses at the level of microzones, we therefore repeated these experiments using two-photon Ca^{2+} imaging using five whiskers that were stimulated individually in a random sequence. To prevent spontaneous whisking and thereby interference from other whiskers, these experiments were (unlike all other experiments in this study) performed under anesthesia. Of the 148 PCs tested, 31 (21%) responded to only one of the five whiskers tested, 14 (10%) to two and 5 (3%) to three whiskers (Figure 5A, B). Not all whiskers were equally effective in recruiting PC responses: 23 cells (15%) responded to C3 stimulation, but only 4 (3%) to C1 stimulation (Table 4). Likewise, pairs of more anterior whiskers had higher chances to be encoded by the same PC (Figure 5C; Table 4).

We also found that PCs can be very specific, responding to a single whisker but not to neighboring whiskers (Figure 5A). We then examined the spatial distribution of responsive PCs. In Figure 5D two nearby recording spots from the same mouse are shown. In recording spot 1, from which the example in Figure 5A originates, all PCs responded to stimulation of at least one whisker. However, in the second recording spot, only two PCs responded, both to a single, but different whisker. For each recording spot we compared responsive vs. non-responsive PCs. This yielded a clear separation for the PCs in the first, but a rather poor one in the second recording spot (Figure 5E). In terms of number of responsive PCs and response amplitudes, these two recordings, although stemming from the same lobule in the same animal, form extreme examples in our dataset. When plotting the response strength versus the fraction of responsive PCs per field of view, we found a positive correlation (linear

regression: R = 0.5208; $p < 0.001$; Figure 5F), implying that PCs with stronger responses to a certain whisker tended to be surrounded by other PCs encoding the same whisker – in line with the much stronger responses in the first than in the second recording spot illustrated in Figure 5D-E. Thus, although our data support the notion that nearby PCs engage in the same sensory module, we could not find clear-cut spatial clusters of PCs encoding the same stimulus.

Stimulus strength has limited impact on complex spike responses

To avoid recruiting responses from adjacent areas, we took care to use weak stimulation strengths (Figures 3-5). Under anesthesia, complex spike response probabilities depend on the stimulation strength (Eccles et al., 1972; Bosman et al., 2010). This finding has been reproduced in awake mice using variations in duration and strength of peri-ocular air puff stimulation (Najafi et al., 2014). Consequently, our approach could have led to an underestimation of the number and spatial extent of climbing fiber responses. To study whether stimulus strength could also have affected our results, we performed an experiment in which we stimulated all whiskers mechanically with three different strengths, the largest of which was identical to the maximal stimulus we previously applied under anesthesia (Bosman et al., 2010). The chosen stimulus intensities maximized the variation in kinetic energy, which was the most salient feature for barrel cortex neurons (Arabzadeh et al., 2004). Stimuli were randomly intermingled (Figure 6A-B). Raw traces indicate that, even at the ensemble level, (relatively) weak stimuli do not trigger responses at every trial (compare Figures 2C and 6C). Of the 340 PCs tested in awake mice, 209 (61%) responded significantly to at least one stimulus strength. In these 209 PCs, we compared the complex spike responses across three intensities. The weak and the moderate intensities (1 mm displacement reached in 62 ms and 2 mm displacement reached in 31 ms, respectively) showed comparable responses and only

the strong stimulus intensity (4 mm reached in 16 ms) evoked more responses ($F(2) = 57.160$, $p < 0.001$, Friedman's test; Figure 6D-F). Despite being eight times faster (129 mm/s instead of 16 mm/s), the strongest stimulus recruited only 28% (measured as peak response) or 34% (measured as integral of whole response period) more complex spikes than the weak stimulus (Figure 6E-F). We therefore conclude that the complex spike response poorly encodes whisker velocity in awake mice.

Functionally equivalent PCs fire coherently

Our single whisker experiments pointed towards a loose clustering of PCs with the same receptive field. As anesthesia could interfere with such analysis, we applied a similar analysis on our awake imaging data. In a representative example of a field of view with 19 dendrites, 12 responded to whisker pad stimulation. These 12 dendrites were located together, although two non-responsive PCs were located in between (Figure 7A). In general, all pairs of PCs that were both responsive to whisker pad stimulation were more spatially clustered and had a higher degree of coherent firing than "heterogeneous pairs" consisting of one responsive and one non-responsive PC (Figure 7B). This even held true for the same pairs recorded in the absence of sensory stimulation (Figure 7C). The coherence was therefore not (only) related to the processing of sensory input, but present throughout the recording. In this case, we defined coherence as firing within the same frame (approx. 40 ms). Firing within 40 ms should still fall within the same subthreshold oscillation cycle of the inferior olive (Khosrovani et al., 2007). This pattern was true for all types of stimulation during the actual application of the stimulation (Figure 7D) and generally, with the exception of upper lip responsive PCs, also for firing the absence of stimulation (Figure 7E). Thus, PCs with the same receptive field are located close, but loosely, together and have a tendency to fire together – even in the absence of the sensory input itself.

Population responses

The relatively weak stimuli triggered complex spike firing in a responsive PC typically in less than 10% of the trials and even a salient stimulus, such as an air puff to the whiskers, does not evoke a complex spike response on every trial (Figure 2). Previous work (e.g., Ozden et al., 2009; Schultz et al., 2009) has demonstrated that sensory encoding is spatially and temporally distributed across neighboring PCs (De Zeeuw et al., 2011). Since there is a 30:1 convergence of PCs to their target neurons in the cerebellar nuclei (Person and Raman, 2011), the number of co-active PCs may control the strength of cerebellar output via rebound firing (Hoebeek et al., 2010; Witter et al., 2013). We studied the basis for complex spike encoding by evaluating the events detected in all PCs within one field of view. To this end, we constructed aggregate peri-stimulus time histograms (PSTHs) counting for each frame the total number of events detected. In response to air puff stimulation, a strong aggregate response was found – and this response was typically formed by the simultaneous activity of many PCs (Romano et al., 2018). The inter-trial intervals, in contrast, seemed to contain activity in individual or a few dendrites (Figure 8A). We compared the observed distribution of simultaneous events with a Poisson distribution based on the same number of spikes. This revealed that simultaneous activity was much higher than could be expected based on a random distribution. In particular, simultaneous events were largely restricted to the response window. Based upon the Poisson distribution, and for this particular field of view, we could have expected maximally three dendrites to be simultaneously active (grey boxes, Figure 8B). These isolated events formed a background level of activity, largely independent of the moments of stimulation. In contrast, the stimulus-induced activity was predominantly carried by the simultaneous activity of multiple dendrites.

In the same field of view, we also tested the response to the tactile stimulation of the whisker pad, a less effective stimulus. Of the 17 dendrites in this field of view, 12 were found

to be responsive to whisker pad stimulation. Although the absolute number of complex spikes evoked by this stimulus was lower than for air puff stimulation, the same principle held true. Individual activity (grey blocks, Figure 8B) remained largely constant, whereas the sensory signal elicited mainly simultaneous activity. Touching the other facial locations did not result in a discernable increase of spikes as evaluated by the aggregate PSTHs. Yet, in this field of view, also upper lip (3 out of 17 cells), lower lip (4 out of 17 cells) and cheek (1 out of 17 cells) were represented. We conclude that, on a micro-circuit level, sensory responses are mainly encoded by simultaneous activity of PCs – and that the density (rather than the strength; see Figure 6) of responsive cells highly promotes signal propagation.

We observed that the spike rate during the inter-trial interval was lower during air puff stimulation than during the other stimulus types. This is apparent when overlaying the air puff-induced aggregate PSTH with that of, for instance, the lower lip (Figure 7C). We quantified this for all nine fields of view tested in this way and found that during the whole recording, the number of complex spike was not significantly different from an equally long recording in the absence of stimulation ($F(2.544, 20.348) = 2.561$, $p = 0.091$, repeated measures ANOVA with Greenhouse-Geisser correction; Figure 8D). Thus, the impact of sensory stimulation seems to be temporal redistribution rather than addition of complex spikes.

Homeostasis of complex spike firing

In Figure 8, we compared the same PCs over various stimulus conditions, irrespective of whether they were responsive to those stimuli. For a further analysis of the temporal aspects of complex spike firing, we restricted our analysis to homogenously responsive PCs only. To study the impact of air puff stimulation, we compared the air puff-induced PSTHs of 117 PCs to their firing pattern during equally long recordings in the absence of sensory stimulation. To

facilitate comparisons, we introduced pseudo-stimuli generated offline with the same 1 Hz rhythm as real stimuli as triggers to create PSTHs. The increase in post-stimulus response came at the expense of a lower firing rate during inter-trial intervals (interval -500 to -250 ms: with stimulation: f = 0.70 ± 0.03 Hz; without stimulation: f = 0.86 ± 0.03 Hz; $t(116) = 3.699$, $p < 0.001$, *t* test; Figure 9). A similar effect was found for a less effective stimulus: whisker pad touches (with stimulation: f = 0.93 ± 0.04 Hz; without stimulation: f = 1.19 ± 0.05 Hz; $t(44) = 6.290$, $p < 0.001$, *t* test). This effect is in line with the differences between responsive and non-responsive cells (Figure 3D).

Visual stimulation induced responses with a longer latency (Figure 3F), which could reflect the different anatomical pathway involved. In Figure 3D, the pre-stimulus interval of visually responsive and non-responsive cells seemed to differ less than for the other types of stimulation. For this reason, we also included visually evoked complex spike responses into our analysis. It appeared that visual stimulation led to a multi-phasic response, which became visible by expanding the time axis. Comparing the interval between 500 and 250 ms prior to the stimulus yielded also a clear reduction in inter-trial firing (with stimulation: f = 1.00 ± 0.05 Hz; without stimulation: f = 1.12 ± 0.03 Hz; $t(26) = 2.624$, $p = 0.0144$, *t* test). Applying Bonferroni correction for multiple comparisons did not affect these conclusions ($\alpha = 0.05 / 3 = 0.017$). Thus, we conclude that various types of stimulation invariably result in a temporal re-ordering of complex spikes.

Discussion

Complex spike firing may appear notoriously unpredictable as its spontaneous frequency is low, yet sustained, and its response rate is at best moderate, with large jitters and an ambiguous relation to stimulus strength. This raises the question as to how the inferior olive relays its signals over time. Possibly, synchronous complex spike firing by neighboring PCs might jointly represent a stimulus, together covering the required signaling for a particular temporal domain (Sasaki et al., 1989; Lang et al., 1999; Sugihara et al., 2007; Ozden et al., 2009; Schultz et al., 2009). Furthermore, the spatial relation between somatotopic patches and parasagittally oriented microzones has not been clarified in terms of complex spike signaling, and it is not understood to what extent this relation also depends on the temporal context in which the signals are generated.

Here, we investigated at the level of individual PCs whether encoding of somatosensory input from different facial areas in lobules crus 1 and 2 occurs in striped microzones or instead follows a more fractured arrangement. Mild touches at localized facial areas revealed a loose version of fractured somatotopy. Tactile input from different locations as well as visual stimulation converged on the same PCs, but not robustly, and complex spikes responding coherently to the stimulus occurred at the expense of those spontaneously occurring during inter-trial intervals. In short, sensory stimulation creates an integrative spatiotemporal pattern consisting of a temporal re-ordering of complex spikes, with increased coherence among functionally equivalent PCs located together, facilitating transmission of salient sensory events.

The functional role of climbing fiber activity

Clinical manifestations of inferior olivary dysfunction range from ataxia and tremor to autism spectrum disorders (Llinás et al., 1975; Samuel et al., 2004; Bauman and Kemper, 2005; Lim and Lim, 2009; De Gruijl et al., 2013). Climbing fiber-evoked complex spikes are also essential for the proper timing, size and direction of movements as well as for the encoding of expected and unexpected deviations from planned movements (Wang et al., 1987; Simpson et al., 1996; Kitazawa et al., 1998; Ito, 2013; Yang and Lisberger, 2014; Herzfeld et al., 2018). In addition, climbing fiber activity is crucial for cerebellar learning by controlling synaptic plasticity at a wide variety of synapses in the molecular layer of the cerebellar cortex (Ito and Kano, 1982; Ito, 2003; Coesmans et al., 2004; Gao et al., 2012). Despite these many functions, complex spike firing is remarkably stable over long intervals, suggesting that the impact of complex spikes is strongly context-dependent.

This context is provided by synaptic inputs to the inferior olive (De Zeeuw et al., 1998), provided by excitatory ascending and descending pathways as well as from inhibitory projections from the hindbrain. Both types converge on spines present on all inferior olivary neurons (De Zeeuw et al., 1989; De Zeeuw et al., 1990). The inhibitory input comes predominantly from the cerebellar nuclei, implying that part of the context is mediated by the target regions of the climbing fibers themselves. This feedback is largely a closed loop, as individual climbing fibers of each olivary subnucleus project to PCs located within a specific parasagittal zone (Sugihara et al., 2001) that converge on particular groups of neurons in the cerebellar nuclei. These neurons project back to the same olivary subnucleus where the loop started (Groenewegen et al., 1979; Voogd and Glickstein, 1998; Apps et al., 2018). Each module can be further subdivided into microzones within which complex spike coherence is clearly enhanced upon strong stimulation (Ozden et al., 2009; Tsutsumi et al., 2015), a phenomenon that is enhanced by strong electrotonic coupling within olivary glomeruli (Sotelo

et al., 1974; Ruigrok et al., 1990; Devor and Yarom, 2002; De Gruijl et al., 2014). Strong stimuli can also increase the coherence of PCs in adjacent bands (Tsutsumi et al., 2015) while our present data show that weak stimuli can trigger responses of loosely grouped cells not encompassing a full microzone. Thus, although anatomical and functional data support the microzonal organization, the activity patterns are best understood as produced dynamically depending on the behavioral context that is transmitted via cerebellar and extra-cerebellar synaptic input.

Receptive fields of PCs and population coding

The existing maps of somatosensory representations of complex spike activity suggest a fractured somatotopy (Miles and Wiesendanger, 1975; Shambes et al., 1978; Rushmer et al., 1980; Castelfranco et al., 1994; Apps and Hawkes, 2009). These maps were typically created by establishing, for each recording position, the strongest input region, disregarding information on convergence of multiple inputs. These studies made clear, however, that climbing fibers could have receptive fields of widely different sizes, expanding to structures as large as a whole limb (Thach, 1967). Part of this can be explained by the sagittally fanning climbing projections onto multiple lobules (Sugihara et al., 2001). Here we show with cellular resolution within cerebellar microzones that climbing fibers indeed do convey somatosensory input from different areas, with PCs having the same receptive fields being located preferably in each other's proximity.

Our data confirm that increasing the stimulus strength promotes complex spike responses, but the impact might be lower than predicted by other studies (Eccles et al., 1972; Bosman et al., 2010; Najafi et al., 2014), showing again the relevance of the behavioral context for complex spike firing. More salient than the stimulus strength might be the combination of sensory inputs, in line with the trend of their convergence on single PCs.

Analyzing the response rates of PC ensembles revealed that the density of responsive cells is crucial for shaping the population response. We propose that the weak spatial clustering of PCs encoding the same stimulus, being interspersed with PCs receiving input from other sources, and the tendency of coherent firing of PCs encoding the same stimulus all contribute to the creation of a heterogeneous map of PCs, where each area encodes a particular functional set of inputs. Each of the properties of the complex spikes seems rather insignificant in isolation, but in combination may result in specific and robust population encoding.

Non-tactile inputs

Light or sound can act as conditional stimulus to recruit increasingly more climbing fiber activity during learning, highlighting the flexibility of this pathway (Ohmae and Medina, 2015; Ten Brinke et al., 2015). We show here that, also in naïve animals, visual and auditory input can converge on the same PCs that encode somatosensory input, further strengthening the notion that climbing fiber activity can act as integrator of contextual input.

In our hands, the auditory response to the sound of the stimulator was highly variable. Comparing the responses to the movement in the presence and absence of skin stimulation revealed that PCs that responded to the sound alone often, but not always, responded to the sound and touch together. The sound that we presented was relatively weak and produced in the noisy environment of a scanning microscope. We therefore assume that perception of the auditory stimulus, more than that of the other stimuli applied, depended on the state of attention of the mice, which highlights the importance of context of complex spike responses.

With visual stimulation the latency was significantly longer than expected. Probably, the presented visual stimulus is not directly relayed from the retina, but a descending input

from the visual cortex or other higher brain regions such as the mesodiencephalic junction (De Zeeuw et al., 1998).

Homeostasis of complex spike frequency

The overall firing rate of complex spikes was stable across conditions, with response peaks being compensated by reduced inter-trial firing. The stronger the response peak, the less inter-trial firing, leading to homeostasis of complex spike firing over longer time periods. Intriguingly, the complex spikes during the inter-trial intervals were predominantly fired by a few, dispersed PCs and the response peak was largely due to increased coherence. It seems therefore that PCs display a basic complex spike firing rate, which in the absence of functional behavior is not coherent with adjacent PCs. In view of the strong impact of complex spikes on synaptic plasticity (Ito and Kano, 1982; Ito, 2003; Coesmans et al., 2004; Gao et al., 2012), this could subserve homeostatic functions. Salient stimuli are largely encoded by coherent firing, making them different from non-stimulus related activity.

Several mechanisms may contribute to the homeostatic control of inferior olivary spiking, including the previously mentioned olivo-cerebellar loops. Disrupted PC activity can affect climbing fiber activity (Chen et al., 2010) and reduced inferior olivary activity leads to enhanced simple spike activity (Montarolo et al., 1982), which in turn dampens activity in the GABAergic neurons of the cerebellar nuclei that controls the inferior olive (Chaumont et al., 2013; Witter et al., 2013). The interplay between glutamatergic input to the neurons of the inferior olive, intracellular signaling and electrotonic coupling may also lead to homeostatic control of complex spike firing via PKA and ßCaMKII (Mathy et al., 2014; Bazzigaluppi et al., 2017). Overall, the inferior olive functions at the cross road of well-defined and rigid anatomical structures and highly dynamic synaptic input, while subject to homeostatic control, the source of which is still to be determined.

References

Albus JS (1971) Theory of cerebellar function. Math Biosci 10:25-61.

Apps R, Garwicz M (2005) Anatomical and physiological foundations of cerebellar information processing. Nat Rev Neurosci 6:297-311.

Apps R, Hawkes R (2009) Cerebellar cortical organization: a one-map hypothesis. Nat Rev Neurosci 10:670-681.

Apps R, Hawkes R, Aoki S, Bengtsson F, Brown AM, Chen G, Ebner TJ, Isope P, Jorntell H, Lackey EP, Lawrenson C, Lumb B, Schonewille M, Sillitoe RV, Spaeth L, Sugihara I, Valera A, Voogd J, Wylie DR, Ruigrok TJH (2018) Cerebellar modules and their role as operational cerebellar processing units. Cerebellum.

Arabzadeh E, Panzeri S, Diamond ME (2004) Whisker vibration information carried by rat barrel cortex neurons. J Neurosci 24:6011-6020.

Axelrad H, Crepel F (1977) Représentation sélective des vibrisses mystaciales au niveau des cellules de Purkinje du cervelet par la voie des fibres grimpantes chez le rat. C R Acad Sci Hebd Seances Acad Sci D 284:1321-1324.

Bauman ML, Kemper TL (2005) Neuroanatomic observations of the brain in autism: a review and future directions. Int J Dev Neurosci 23:183-187.

Bazzigaluppi P, Isenia SC, Haasdijk ED, Elgersma Y, De Zeeuw CI, van der Giessen RS, de Jeu MTG (2017) Modulation of murine olivary connexin 36 gap Junctions by PKA and CaMKII. Front Cell Neurosci 11:397.

Bloedel JR, Ebner TJ (1984) Rhythmic discharge of climbing fibre afferents in response to natural peripheral stimuli in the cat. J Physiol 352:129-146.

Bosman LWJ, Koekkoek SKE, Shapiro J, Rijken BFM, Zandstra F, van der Ende B, Owens CB, Potters JW, de Gruijl JR, Ruigrok TJH, De Zeeuw CI (2010) Encoding of whisker input by cerebellar Purkinje cells. J Physiol 588:3757-3783.

Bosman LWJ, Houweling AR, Owens CB, Tanke N, Shevchouk OT, Rahmati N, Teunissen WHT, Ju C, Gong W, Koekkoek SKE, De Zeeuw CI (2011) Anatomical pathways involved in generating and sensing rhythmic whisker movements. Front Integr Neurosci 5:53.

Brown IE, Bower JM (2002) The influence of somatosensory cortex on climbing fiber responses in the lateral hemispheres of the rat cerebellum after peripheral tactile stimulation. J Neurosci 22:6819-6829.

Brown ST, Raman IM (2018) Sensorimotor integration and amplification of reflexive whisking by well-timed spiking in the cerebellar corticonuclear circuit. Neuron (in press).

Castelfranco AM, Robertson LT, McCollum G (1994) Detail, proportion, and foci among face receptive fields of climbing fiber responses in the cat cerebellum. Somatosens Mot Res 11:27-46.

Cerminara NL, Lang EJ, Sillitoe RV, Apps R (2015) Redefining the cerebellar cortex as an assembly of non-uniform Purkinje cell microcircuits. Nat Rev Neurosci 16:79-93.

Chaplan SR, Bach FW, Pogrel JW, Chung JM, Yaksh TL (1994) Quantitative assessment of tactile allodynia in the rat paw. J Neurosci Methods 53:55-63.

Chaumont J, Guyon N, Valera AM, Dugué GP, Popa D, Marcaggi P, Gautheron V, Reibel-Foisset S, Dieudonné S, Stephan A, Barrot M, Cassel JC, Dupont JL, Doussau F, Poulain B, Selimi F, Léna C, Isope P (2013) Clusters of cerebellar Purkinje cells control their afferent climbing fiber discharge. Proc Natl Acad Sci U S A 110:16223-16228.

Chen X, Kovalchuk Y, Adelsberger H, Henning HA, Sausbier M, Wietzorrek G, Ruth P, Yarom Y, Konnerth A (2010) Disruption of the olivo-cerebellar circuit by Purkinje neuron-specific ablation of BK channels. Proc Natl Acad Sci U S A 107:12323-12328.

Coesmans M, Weber JT, De Zeeuw CI, Hansel C (2004) Bidirectional parallel fiber plasticity in the cerebellum under climbing fiber control. Neuron 44:691-700.

De Gruijl JR, Hoogland TM, De Zeeuw CI (2014) Behavioral correlates of complex spike synchrony in cerebellar microzones. J Neurosci 34:8937-8944.

De Gruijl JR, Bosman LWJ, De Zeeuw CI, De Jeu MTG (2013) Inferior olive: All ins and outs. In: Handbook of the Cerebellum and Cerebellar Disorders (Manto M, Schmahmann JD, Rossi F, Gruol DL, Koibuchi N, eds), pp 1013-1058. Dordrecht: Springer Netherlands.

De Zeeuw CI, Ten Brinke MM (2015) Motor learning and the cerebellum. Cold Spring Harb Perspect Biol 7:a021683.

De Zeeuw CI, Hertzberg EL, Mugnaini E (1995) The dendritic lamellar body: a new neuronal organelle putatively associated with dendrodendritic gap junctions. J Neurosci 15:1587-1604.

De Zeeuw CI, Holstege JC, Ruigrok TJ, Voogd J (1989) Ultrastructural study of the GABAergic, cerebellar, and mesodiencephalic innervation of the cat medial accessory olive: anterograde tracing combined with immunocytochemistry. J Comp Neurol 284:12-35.

De Zeeuw CI, Holstege JC, Ruigrok TJH, Voogd J (1990) Mesodiencephalic and cerebellar terminals terminate upon the same dendritic spines in the glomeruli of the cat and rat inferior olive: an ultrastructural study using a combination of [^{3}H]leucine and wheat germ agglutinin coupled horseradish peroxidase anterograde tracing. Neuroscience 34:645-655.

De Zeeuw CI, Simpson JI, Hoogenraad CC, Galjart N, Koekkoek SKE, Ruigrok TJH (1998) Microcircuitry and function of the inferior olive. Trends Neurosci 21:391-400.

De Zeeuw CI, Hoebeek FE, Bosman LWJ, Schonewille M, Witter L, Koekkoek SK (2011) Spatiotemporal firing patterns in the cerebellum. Nat Rev Neurosci 12:327-344.

Devor A, Yarom Y (2002) Electrotonic coupling in the inferior olivary nucleus revealed by simultaneous double patch recordings. J Neurophysiol 87:3048-3058.

Eccles JC, Sabah NH, Schmidt RF, Táboríková H (1972) Cutaneous mechanoreceptors influencing impulse discharges in cerebellar cortex. III. In Purkyně cells by climbing fiber input. Exp Brain Res 15:484-497.

Ekerot CF, Garwicz M, Schouenborg J (1991) Topography and nociceptive receptive fields of climbing fibres projecting to the cerebellar anterior lobe in the cat. J Physiol 441:257-274.

Gao Z, Van Beugen BJ, De Zeeuw CI (2012) Distributed synergistic plasticity and cerebellar learning. Nat Rev Neurosci 13:619-635.

Gibson AR, Horn KM, Pong M (2004) Activation of climbing fibers. Cerebellum 3:212-221.

Groenewegen HJ, Voogd J, Freedman SL (1979) The parasagittal zonation within the olivocerebellar projection. II. Climbing fiber distribution in the intermediate and hemispheric parts of cat cerebellum. J Comp Neurol 183:551-601.

Harvey RJ, Napper RMA (1991) Quantitative studies on the mammalian cerebellum. Prog Neurobiol 36:437-463.

Herzfeld DJ, Kojima Y, Soetedjo R, Shadmehr R (2018) Encoding of error and learning to correct that error by the Purkinje cells of the cerebellum. Nat Neurosci 21:736-743.

Hoebeek FE, Witter L, Ruigrok TJH, De Zeeuw CI (2010) Differential olivo-cerebellar cortical control of rebound activity in the cerebellar nuclei. Proc Natl Acad Sci U S A 107:8410-8415.

Hoogland TM, De Gruijl JR, Witter L, Canto CB, De Zeeuw CI (2015) Role of synchronous activation of cerebellar Purkinje cell ensembles in multi-joint movement control. Curr Biol 25:1157-1165.

Ito M (2003) Long-term depression. Annu Rev Neurosci 12:85-102.

Ito M (2013) Error detection and representation in the olivo-cerebellar system. Front Neural Circuits 7:1.

Ito M, Kano M (1982) Long-lasting depression of parallel fiber-Purkinje cell transmission induced by conjunctive stimulation of parallel fibers and climbing fibers in the cerebellar cortex. Neurosci Lett 33:253-258.

Joseph JW, Shambes GM, Gibson JM, Welker W (1978) Tactile projections to granule cells in caudal vermis of the rat's cerebellum. Brain Behav Evol 15:141-149.

Keser Z, Hasan KM, Mwangi BI, Kamali A, Ucisik-Keser FE, Riascos RF, Yozbatiran N, Francisco GE, Narayana PA (2015) Diffusion tensor imaging of the human cerebellar pathways and their interplay with cerebral macrostructure. Front Neuroanat 9:41.

Khosrovani S, Van Der Giessen RS, De Zeeuw CI, De Jeu MTG (2007) *In vivo* mouse inferior olive neurons exhibit heterogeneous subthreshold oscillations and spiking patterns. Proc Natl Acad Sci U S A 104:15911-15916.

Kitazawa S, Kimura T, Yin PB (1998) Cerebellar complex spikes encode both destinations and errors in arm movements. Nature 392:494-497.

Kubo R, Aiba A, Hashimoto K (2018) The anatomical pathway from the mesodiencephalic junction to the inferior olive relays perioral sensory signals to the cerebellum in the mouse. J Physiol (in press).

Lang EJ, Sugihara I, Welsh JP, Llinás R (1999) Patterns of spontaneous purkinje cell complex spike activity in the awake rat. J Neurosci 19:2728-2739.

Lim CCT, Lim SA (2009) Pendular nystagmus and palatomyoclonus from hypertrophic olivary degeneration. New Engl J Med 360:e12.

Llinás R, Walton K, Hillman DE, Sotelo C (1975) Inferior olive: its role in motor learing. Science 190:1230-1231.

Mathy A, Clark BA, Häusser M (2014) Synaptically induced long-term modulation of electrical coupling in the inferior olive. Neuron 81:1290-1296.

Miles TS, Wiesendanger M (1975) Organization of climbing fibre projections to the cerebellar cortex from trigeminal cutaneous afferents and from the SI face area of the cerebral cortex in the cat. J Physiol 245:409-424.

Montarolo PG, Palestini M, Strata P (1982) The inhibitory effect of the olivocerebellar input on the cerebellar Purkinje cells in the rat. J Physiol 332:187-202.

Mukamel EA, Nimmerjahn A, Schnitzer MJ (2009) Automated analysis of cellular signals from large-scale calcium imaging data. Neuron 63:747-760.

Najafi F, Giovannucci A, Wang SSH, Medina JF (2014) Coding of stimulus strength via analog calcium signals in Purkinje cell dendrites of awake mice. eLIFE 3:e03663.

Ohmae S, Medina JF (2015) Climbing fibers encode a temporal-difference prediction error during cerebellar learning in mice. Nat Neurosci 18:1798-1803.

Oscarsson O (1969) Termination and functional organization of the dorsal spino-olivocerebellar path. J Physiol 200:129-149.

Ozden I, Sullivan MR, Lee HM, Wang SSH (2009) Reliable coding emerges from coactivation of climbing fibers in microbands of cerebellar Purkinje neurons. J Neurosci 29:10463-10473.

Ozden I, Dombeck DA, Hoogland TM, Tank DW, Wang SS (2012) Widespread state-dependent shifts in cerebellar activity in locomoting mice. PLoS One 7:e42650.

Person AL, Raman IM (2011) Purkinje neuron synchrony elicits time-locked spiking in the cerebellar nuclei. Nature 481:502-505.

Peter S, Ten Brinke MM, Stedehouder J, Reinelt CM, Wu B, Zhou H, Zhou K, Boele HJ, Kushner SA, Lee MG, Schmeisser MJ, Boeckers TM, Schonewille M, Hoebeek FE, De Zeeuw CI (2016) Dysfunctional cerebellar Purkinje cells contribute to autism-like behaviour in *Shank2*-deficient mice. Nat Commun 7:12627.

Rahmati N, Owens CB, Bosman LWJ, Spanke JK, Lindeman S, Gong W, Potters JW, Romano V, Voges K, Moscato L, Koekkoek SKE, Negrello M, De Zeeuw CI (2014) Cerebellar potentiation and learning a whisker-based object localization task with a time response window. J Neurosci 34:1949-1962.

Robertson LT, Laxer KD, Rushmer DS (1982) Organization of climbing fiber input from mechanoreceptors to lobule V vermal cortex of the cat. Exp Brain Res 46:281-291.

Romano V, De Propris L, Bosman LWJ, Warnaar P, Ten Brinke MM, Lindeman S, Ju C, Velauthapillai A, Spanke JK, Middendorp Guerra E, Hoogland TM, Negrello M, D'Angelo E, De Zeeuw CI (2018) Adaptation of whisker movements requires cerebellar potentiation. bioRxiv:335489.

Ruigrok TJH, de Zeeuw CI, van der Burg J, Voogd J (1990) Intracellular labeling of neurons in the medial accessory olive of the cat: I. Physiology and light microscopy. J Comp Neurol 300:462-477.

Rushmer DS, Woollacott MH, Robertson LT, Laxer KD (1980) Somatotopic organization of climbing fiber projections from low threshold cutaneous afferents to pars intermedia of cerebellar cortex in the cat. Brain Res 181:17-30.

Samuel M, Torun N, Tuite PJ, Sharpe JA, Lang AE (2004) Progressive ataxia and palatal tremor (PAPT): clinical and MRI assessment with review of palatal tremors. Brain 127:1252-1268.

Sasaki K, Bower JM, Llinás R (1989) Multiple Purkinje cell recording in rodent cerebellar cortex. Eur J Neurosci 1:572-586.

Schäfer CB, Hoebeek FE (2018) Convergence of primary sensory cortex and cerebellar nuclei pathways in the whisker system. Neuroscience 368:229-239.

Schmahmann JD (2004) Disorders of the cerebellum: ataxia, dysmetria of thought, and the cerebellar cognitive affective syndrome. J Neuropsychiatry Clin Neurosci 16:367-378.

Schultz SR, Kitamura K, Post-Uiterweer A, Krupic J, Häusser M (2009) Spatial pattern coding of sensory information by climbing fiber-evoked calcium signals in networks of neighboring cerebellar Purkinje cells. J Neurosci 29:8005-8015.

Shambes GM, Gibson JM, Welker W (1978) Fractured somatotopy in granule cell tactile areas of rat cerebellar hemispheres revealed by micromapping. Brain Behav Evol 15:94-140.

Simpson JI, Wylie DR, De Zeeuw CI (1996) On climbing fiber signals and their consequence(s). Behav Brain Sci 19:384-398.

Sotelo C, Llinás R, Baker R (1974) Structural study of inferior olivary nucleus of the cat: morphological correlates of electrotonic coupling. J Neurophysiol 37:541-559.

Stosiek C, Garaschuk O, Holthoff K, Konnerth A (2003) *In vivo* two-photon calcium imaging of neuronal networks. Proc Natl Acad Sci U S A 100:7319-7324.

Streng ML, Popa LS, Ebner TJ (2017) Climbing fibers predict movement kinematics and performance errors. J Neurophysiol 118:1888-1902.

Sugihara I, Wu HS, Shinoda Y (2001) The entire trajectories of single olivocerebellar axons in the cerebellar cortex and their contribution to cerebellar compartmentalization. J Neurosci 21:7715-7723.

Sugihara I, Marshall SP, Lang EJ (2007) Relationship of complex spike synchrony bands and climbing fiber projection determined by reference to aldolase C compartments in crus IIa of the rat cerebellar cortex. J Comp Neurol 501:13-29.

Tada M, Takeuchi A, Hashizume M, Kitamura K, Kano M (2014) A highly sensitive fluorescent indicator dye for calcium imaging of neural activity *in vitro* and *in vivo*. Eur J Neurosci 39:1720-1728.

Ten Brinke MM, Boele HJ, Spanke JK, Potters JW, Kornysheva K, Wulff P, IJpelaar ACHG, Koekkoek SKE, De Zeeuw CI (2015) Evolving models of Pavlovian conditioning: cerebellar cortical dynamics in awake behaving mice. Cell Rep 13:1977-1988.

Thach WT, Jr. (1967) Somatosensory receptive fields of single units in cat cerebellar cortex. J Neurophysiol 30:675-696.

Tsutsumi S, Yamazaki M, Miyazaki T, Watanabe M, Sakimura K, Kano M, Kitamura K (2015) Structure-function relationships between aldolase C/zebrin II expression and complex spike synchrony in the cerebellum. J Neurosci 35:843-852.

Van Der Giessen RS, Koekkoek SK, van Dorp S, De Gruijl JR, Cupido A, Khosrovani S, Dortland B, Wellershaus K, Degen J, Deuchars J, Fuchs EC, Monyer H, Willecke K, De Jeu MTG, De Zeeuw CI (2008) Role of olivary electrical coupling in cerebellar motor learning. Neuron 58:599-612.

Voogd J, Glickstein M (1998) The anatomy of the cerebellum. Trends Neurosci 21:370-375.

Wang JJ, Kim JH, Ebner TJ (1987) Climbing fiber afferent modulation during a visually guided, multi-joint arm movement in the monkey. Brain Res 410:323-329.

Welsh JP, Lang EJ, Suglhara I, Llinas R (1995) Dynamic organization of motor control within the olivocerebellar system. Nature 374:453-457.

Witter L, Canto CB, Hoogland TM, de Gruijl JR, De Zeeuw CI (2013) Strength and timing of motor responses mediated by rebound firing in the cerebellar nuclei after Purkinje cell activation. Front Neural Circuits 7:133.

Xiao J, Cerminara NL, Kotsurovskyy Y, Aoki H, Burroughs A, Wise AK, Luo Y, Marshall SP, Sugihara I, Apps R, Lang EJ (2014) Systematic regional variations in Purkinje cell spiking patterns. PLoS One 9:e105633.

Yang Y, Lisberger SG (2014) Purkinje-cell plasticity and cerebellar motor learning are graded by complex-spike duration. Nature 510:529-532.

Yatim N, Billig I, Compoint C, Buisseret P, Buisseret-Delmas C (1996) Trigeminocerebellar and trigemino-olivary projections in rats. Neurosci Res 25:267-283.

Zhou H, Lin Z, Voges K, Ju C, Gao Z, Bosman LWJ, Ruigrok TJH, Hoebeek FE, De Zeeuw CI, Schonewille M (2014) Cerebellar modules operate at different frequencies. eLIFE 3:e02536.

Figure legends

Figure 1 – Sensory pathways carrying facial input to the cerebellar cortex

Simplified scheme of the main routes conveying facial tactile input via the climbing fiber pathway to cerebellar PCs. Climbing fibers, which cause complex spike firing in PCs, exclusively originate from the inferior olive. The inferior olive is directly innervated by neurons from the trigeminal nuclei as well as indirectly via thalamo-cortical pathways that project to the inferior olive mainly via the nuclei of the meso-diencephalic junction (MDJ). The MDJ itself also receives direct input from the trigeminal nuclei. See the main text for references.

Figure 2 - Whisker stimulation evokes complex spike responses in cerebellar crus 1 and crus 2 (A) Complex spikes elicit large increases in the Ca^{2+} concentration within PC dendrites that can be resolved using *in vivo* two-photon microscopy in combination with fluorescent Ca^{2+} indicators. An example of 19 identified PC dendrites is shown with each individual dendrite denoted by a unique color. **(C)** Summed fluorescence trace composed of all 19 individual traces emphasizing the participation of many PCs to the stimulus-triggered responses. **(D)** The fluorescent traces of each of these dendrites show distinct Ca^{2+} transient events, which are to a large extent associated with air puff stimulation of the facial whiskers (times of stimulation indicated by the vertical lines). **(E)** Peri-stimulus time histogram of one of the PCs indicated above in response to air puff stimulation to the ipsilateral whiskers. The bin size (40 ms) corresponds to the acquisition frame rate (25 Hz). **(F)** Normalized stacked line graph of the PCs in this field of view showing that each of these cells contributed to the overall response. The colors match those in the panels B-D. *Inset:* In total, we found that 102 out of 118 cells analyzed (86%) were responsive to whisker air puff stimulation.

Figure 3 – PCs in crus 1 and crus 2 respond to various types of sensory stimulation

(A) We presented tactile stimuli to four facial regions in awake mice: the whisker pad, the upper lip, the lower lip and the cheek. Each stimulus was delivered with a piezo-actuator that made a muted, yet audible sound which was also delivered without touch ("sound"). A blue light flash generated by an LED was used as visual stimulus. **(B)** To avoid interference of adjacent areas, we applied very gentle touches (0.686 mN). The complex spike response ratio was much reduced relative to the strong air puff stimulation to all ipsilateral whiskers illustrated in Figure 2. A fluorescent trace from a representative PC shows that responses to whisker pad stimulation could be evoked even with gentle stimulation. Sensory responses for all stimulus conditions in this cell are further illustrated by peri-stimulus time histograms (PSTHs) (**C**). This particular PC responded to whisker pad, upper lip, lower lip and visual stimulation. Significance was calculated using a bootstrap method, with the black line representing the expected firing rate and the dashed line the average + 2 s.d. **(D)** For each stimulus condition, we averaged the PSTHs for all PCs that were responsive to that particular stimulus (*colored lines*; averages ± SEM). These were contrasted to the averaged PSTH of all non-responsive PCs (*black lines*; averages ± SEM). The pie charts represent the fraction of PCs responsive to each particular stimulus. **(E)** The peak responses were the lowest for sound and for upper lip stimulation. * $p < 0.05$; ** $p < 0.01$ (post-hoc tests after Kruskal-Wallis test) **(F)** As expected for complex spike responses to weak stimulation, the latencies were relatively long and variable, but consistent across types of stimulation. Only visual stimulation (LED) had a remarkably longer latency time. *** $p < 0.001$ (post-hoc tests after Kruskal-Wallis test for LED vs. whisker pad, upper lip, lower lip and cheek and $p < 0.05$ compared to sound)

Figure 4 – Convergence of sensory input on PCs in crus 1 and crus 2

(A) PCs respond to multiple sources of sensory input (cf. Figure 3). We used a bootstrap method to evaluate whether PCs had a tendency towards segregating or integrating input from different sources. Venn diagram areas correspond to the fraction of PCs responsive to a particular stimulus. The rectangles are proportional to the *Z* score of the overlapping fraction (see scale bar). Grey bars denote a trend ($p < 0.10$) and black bars a significant convergence ($p < 0.05$). **(B)** Auditory and tactile stimuli had more overlap, as could be expected since tactile stimulation was always associated with the sound of the stimulator. The overlap was not complete, however, which might have been due to masking of the stimulator sound by high levels of ambient noise in the room. **(C)** Remarkably, visual and tactile input tended to converge, showing a preference of PCs for multi-modal input. $^{\#}$ $p < 0.10$; * $p < 0.05$ and ** $p < 0.01$ after bootstrap analysis

Figure 5 – PC responses to single whisker stimulation show weak clustering

(A) To investigate even smaller receptive fields, we stimulated sequentially five of the large facial whiskers. To avoid interference with other whiskers during active movement, we performed these experiments under ketamine/xylazine anesthesia. Most PCs, if responsive to single-whisker stimulation, responded only to one of the five whiskers (**B**). This is illustrated by five peri-stimulus time histograms (PSTHs) from a single, representative PC. This particular PC was sensitive to stimulation of the C3 whisker only. The average and 3 s.d. of the baseline firing are indicated (dashed line and grey area). **(C)** PCs that responded to more than one whisker were typically responsive to the more anterior whiskers (see also Table 4). The widths of the lines indicate the *Z* value of the occurrence of multiple responses per cell. **(D)** Two recording spots, located close together in crus 1 of the same mouse, with the identified PC dendritic trees (pseudo-colored in *top row*). For each dendrite, the *bottom row*

shows, in a different color coding scheme (see below the panels), the whisker(s) to which it was responsive (grey indicates no responses). **(E)** For each region, the average (± s.d.) of the responsive and the non-responsive PCs was indicated (to the C3 whisker in the *left panel* and to the C2 whisker in the *right panel*). Note that only a single cell was responsive in recording spot 2. The firing pattern of the non-responsive cells was also averaged (*black shades*). **(F)** Linear regression revealed that PCs that were surrounded by other PCs responsive to the same whisker (same color code as in **A**) had a tendency to show stronger responses to stimulation of that whisker than PCs that were more isolated. The *x*-axis represents the fraction of PCs responsive to the particular whisker within the respective field of view. $R = 0.521$; $p < 0.001$.

Figure 6 – Stimulus strength has only a minor impact on complex spike responsiveness

(A) Movements of all large facial whiskers were performed using a piezo-actuator at three different speeds (weak: 1 mm displacement in 62 ms; moderate: 2 mm displacement in 31 ms; strong: 4 mm displacement in 16 ms). The stimulus sequence was randomly permuted. **(B)** Field of view with 24 identified and color coded PCs (*left*) and their fluorescent traces (*right*). Stimuli were presented every 2 s and in between trials the laser illumination was briefly blocked to avoid photobleaching. The vertical shaded areas indicate the duration of the stimulus (which was inverse with the stimulus strength). **(C)** Summed fluorescence trace composed of all 24 individual traces showing that not all trials evoked ensemble-wide responses. **(D)** The average number of complex spikes per frame (of 40 ms) per trial (shaded areas: ± SEM) for the three stimulus strengths show little difference for the weak and moderate stimulation. The time course and amplitude (1-4 mm) of the three stimuli is schematized at the bottom of the graph. The strong stimulation elicits approx. 30% more complex spikes, as evident from the peak responses for each stimulus intensity **(E)**. The PCs that showed increased responsiveness to stronger stimuli are depicted in red and the others in

blue. **(F)** The same data summarized with box plots for all responsive cells. Data are from 209 responsive PCs (out of 340 PCs that were measured in this way). *** $p < 0.001$ (Friedman's test).

Figure 7 – PCs encoding the same response are closer together

(A) Representative field of view with segmented Purkinje cell dendrites. Non-responsive cells are depicted in shades of blue and responsive cells in shades of red during whisker pad stimulation. **(B)** For each pair of PCs we calculated the correlation coefficient (R) during 1 Hz whisker pad stimulation. The pairs of two PCs that were both responsive to whisker pad stimulation had on average a higher level of coherence than the pairs connecting a responsive and a non-responsive PC ($p < 0.001$; two-dimensional Kolmogorov-Smirnov test). The pairs consisting of two non-responsive PCs were excluded from this analysis. **(C)** Interestingly, even in the absence of sensory stimulation, the pairs of PCs that were both responsive to whisker pad stimulation maintained a higher level of coherence than "heterogeneous pairs". Thus, PCs with the same receptive field tended to fire more coherently, even in the absence of stimulation. This analysis was expanded in the presence (**D**) and absence (**E**) of sensory stimulation for six different types of stimulation and illustrated as the median R value per distance category (six bin values of equal distance at a log scale). The shaded areas represent the inter-quartile ranges. * $p < 0.05$; *** $p < 0.001$ (Kolmogorov-Smirnov tests)

Figure 8 – PCs encode strong and weak sensory stimulation via synchronous firing

(A) Aggregate peri-stimulus time histograms (PSTHs) show that coherent firing of complex spikes predominantly occurs following sensory stimulation. For each field of view, we calculated the number of complex spikes occurring per frame. Subsequently, we made aggregate PSTHs where the color of each bin refers to the number of dendrites simultaneously

active. In this field of view, 17 PCs were measured. Of these, 17 (100%) reacted to air puff, 12 (71%) to whisker pad, 3 (18%) to upper lip, 4 (24%) to lower lip and 1 (6%) to cheek stimulation. **(B)** Based upon a Poisson distribution of complex spikes over all dendrites and bins, one would expect between 0 and 3 simultaneously active dendrites (*grey bars*). The *red bars* indicate events involving more dendrites simultaneously than expected from a random distribution. Thus, the sparse firing as expected by chance is relatively constant throughout the trials, but the simultaneous activity of multiple dendrites is strongly enhanced following sensory stimulation. **(C)** A direct overlay of the aggregate PSTHs in response to air puff and lower lip stimulation shows that the strong response found after air puff stimulation comes at the expense of inter-trial complex spikes (152 trials per condition). **(D)** For equally long recordings in the presence of different types of stimulation, equal complex spike frequencies were observed as during spontaneous activity ($F(2.544, 20.348) = 2.561$, $p = 0.091$, repeated measures ANOVA), indicating that sensory stimulation results in a temporal re-ordering of complex spikes, rather than to the production of more complex spikes.

Figure 9 – Sensory stimulation results in a temporal re-ordering of complex spikes

The temporal distribution of complex spikes was compared between periods with sensory stimulation and periods without. For this analysis, we included only PCs that displayed a significant response to the stimulus involved ($n = 117$ for air puff, $n = 45$ for whisker pad and $n = 27$ for visual stimulation). Irrespective of the type of stimulation, a reduction in inter-trial activity was found. This was quantified by during the period between 500 and 250 ms prior to stimulus onset using paired *t* tests; * and *** indicate $p < 0.05$ and $p < 0.001$, respectively.

Table 1

Stimulation	Responsive cells		Response parameters		Prevalence (*p*) χ^2 = 21.049; df = 5; *p* = 0.001				
	No.	**%**	**Peak (Z)**	**Latency (ms)**	**UL**	**LL**	**CH**	**SO**	**LED**
Whisker pad	111(264)	42	4.09±1.73	84±42	**0.002**	0.328	**0.000**	**0.003**	0.135
Upper lip	71(249)	29	3.68±1.43	84±84		**0.031**	0.597	0.820	0.255
Lower lip	99(264)	38	4.50±2.28	84±42			**0.010**	**0.041**	0.517
Cheek	53(203)	26	4.51±2.30	84±42				0.810	0.119
Sound only	42(154)	27	3.81±1.07	84±84					0.255
LED	48(141)	34	4.28±2.88	126±0					

Table 1 – PC responses to sensory stimulation in awake mice

PCs respond with complex firing to sensory stimulation (cf. Figure 2). For each type of stimulation, the number and percentage of responsive cells is indicated (in brackets: total number of cells tested). The response peak and response latency are indicated as medians ± inter-quartile ranges. The relative prevalence of responses was not equal for all stimulus types, as confirmed by a 6x2 χ^2 test. Differences in relative prevalence were tested using pair-wise Fisher's exact tests. Bold values indicate significantly different prevalences.

Table 2

Stimulation	Rate of occurrence (*Z*)					Chance of occurrence (*p*)				
	UL	LL	CH	SO	LED	UL	LL	CH	SO	LED
Whisker pad	1.21	1.25	0.85	1.34	**2.75**	0.225	0.213	0.394	0.181	**0.006**
Upper lip		1.23	**2.00**	1.34	1.94		0.220	**0.045**	0.181	0.052
Lower lip			**2.39**	**2.70**	**2.62**			**0.017**	**0.007**	**0.009**
Cheek				**3.31**	**3.10**				**0.001**	**0.002**
Sound only					**2.28**					**0.022**

Table 2 – Convergence of different sensory streams on individual PCs

For each type of stimulus, we compared the observed rate of convergence on individual PCs to chance level, using a bootstrap methods based on the relative prevalence of each stimulus (cf. Figure 3). Indicated are the *Z* and the *p* values. All combinations occurred more often than expected ($Z > 0$). Bold values indicate statistical significance.

Table 3

Stimulation	Rate of occurrence (*Z*)	Chance of occurrence (*p*)
WP + UL + LL	1.89	0.059
WP + LL + CH	1.32	0.186
UL + LL + CH	3.22	**0.001**
WP + UL + LL + CH	3.07	**0.002**

Table 3 – Convergence of different sensory streams on individual PCs

For each type of stimulus, we compared the observed rate of convergence on individual PCs to chance level, using a bootstrap methods based on the relative prevalence of each stimulus (cf. Figure 3). Indicated are the *Z* and the *p* values. All combinations occurred more often than expected ($Z > 0$). Bold values indicate statistical significance. WP = whisker pad; UL = upper lip; LL = lower lip; CH = cheek.

Table 4

Whisker	Responsive cells		Rate of occurrence (*Z*)				Prevalence (*p*)			
	No.	**%**	**C1**	**C2**	**C3**	**D2**	**C1**	**C2**	**C3**	**D2**
B2	15 (148)	10	0.630	0.227	**5.130**	**2.052**	0.264	0.410	**<0.001**	**0.020**
C1	4 (148)	3		0.803	0.782	0.630		0.211	0.217	0.264
C2	17 (148)	11			0.222	0.208			0.412	0.418
C3	23 (148)	16				**3.100**				**0.001**
D2	15 (148)	10								

Table 4 – PC responses to single-whisker stimulation in anesthetized mice

PCs respond with complex firing to single-whisker stimulation (cf. Figure 4). For each whisker, the number and percentage of responsive cells is indicated (in brackets: total number of cells tested). For each whisker, we compared the observed rate of convergence on individual PCs to chance level, using a bootstrap methods based on the relative prevalence of each stimulus. Indicated are the *Z* and the *p* values. All combinations occurred more often than expected ($Z > 0$). Bold values indicate statistical significance.

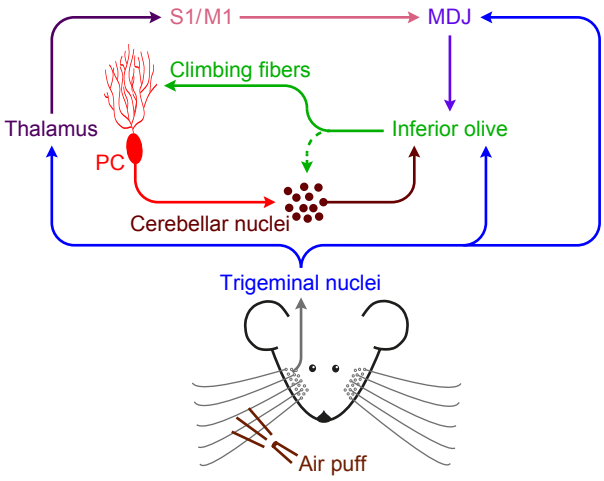

Figure 1 – Sensory pathways carrying facial input to the cerebellar cortex
Simplified scheme of the main routes conveying facial tactile input via the climbing fiber pathway to cerebellar PCs. Climbing fibers, which cause complex spike firing in PCs, exclusively originate from the inferior olive. The inferior olive is directly innervated by neurons from the trigeminal nuclei as well as indirectly via thalamo-cortical pathways that project to the inferior olive mainly via the nuclei of the meso-diencephalic junction (MDJ). The MDJ itself also receives direct input from the trigeminal nuclei. See the main text for references.

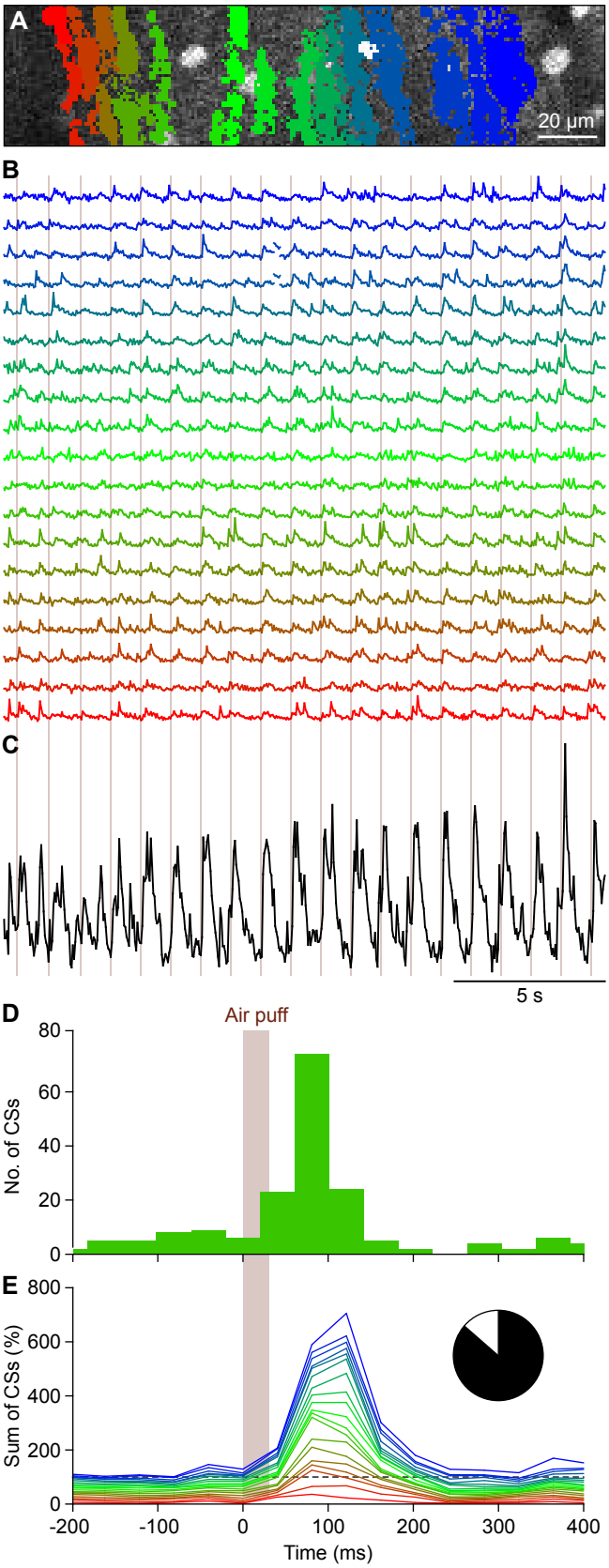

Figure 2 - Whisker stimulation evokes complex spike responses in cerebellar crus 1 and crus 2

(A) Complex spikes elicit large increases in the Ca^{2+} concentration within PC dendrites that can be resolved using *in vivo* two-photon microscopy in combination with fluorescent Ca^{2+} indicators. An example of 19 identified PC dendrites is shown with each individual dendrite denoted by a unique color. **(B)** The fluorescent traces of each of these dendrites show distinct Ca^{2+} transient events, which are to a large extent associated with air puff stimulation of the facial whiskers (times of stimulation indicated by the vertical lines). **(C)** Summed fluorescence trace composed of all 19 individual traces emphasizing the participation of many PCs to the stimulus-triggered responses. **(D)** Peri-stimulus time histogram of one of the PCs indicated above in response to air puff stimulation to the ipsilateral whiskers. The bin size (40 ms) corresponds to the acquisition frame rate (25 Hz) and the color corresponds to the region of interest in **A**. **(E)** Normalized stacked line graph of the PCs in this field of view showing that each of these cells contributed to the overall response. The colors match those in the panels A-B. *Inset:* In total, we found that 102 out of 118 cells analyzed (86%) were responsive to whisker air puff stimulation.

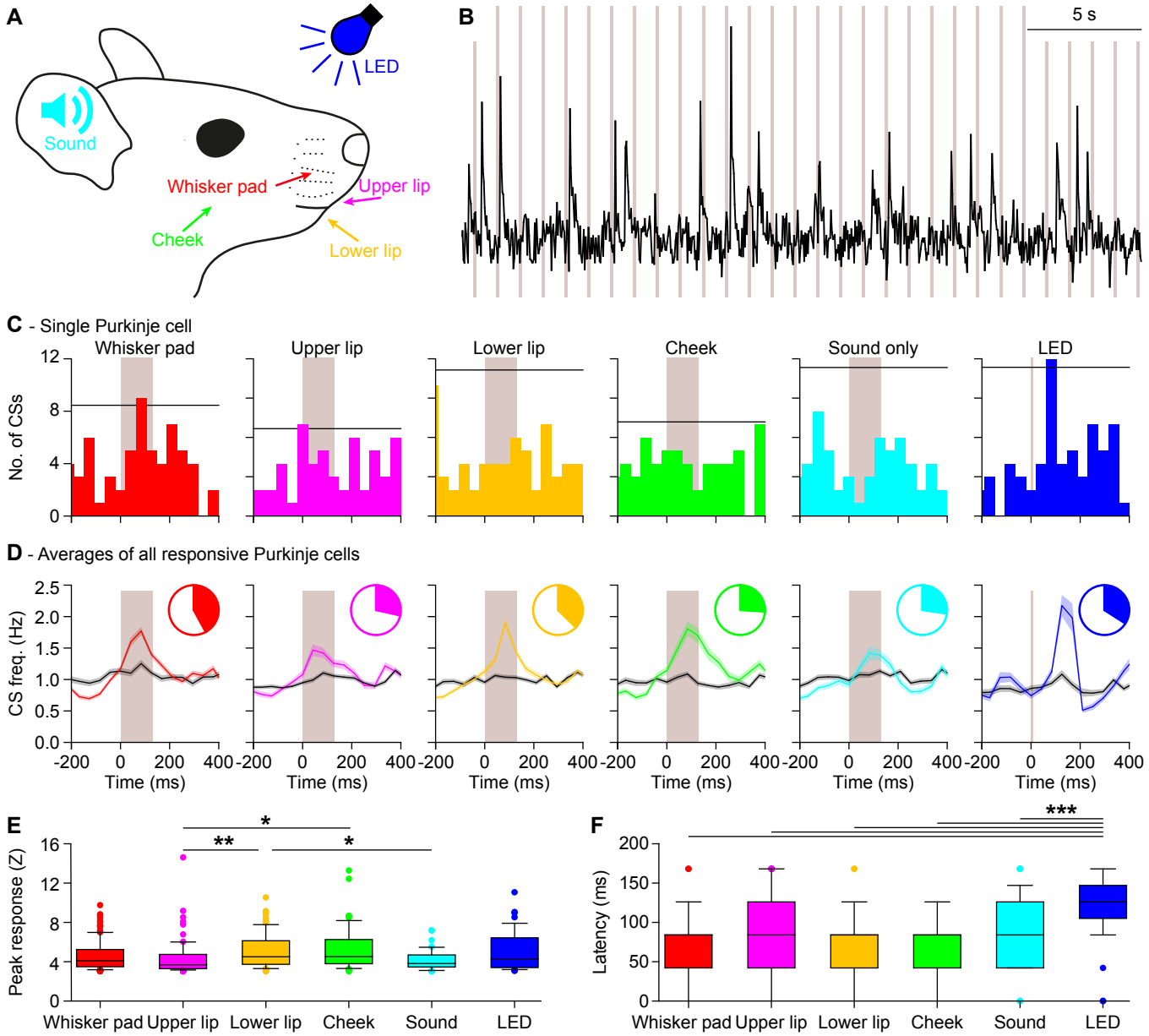

Figure 3 – PCs in crus 1 and crus 2 respond to various types of sensory stimulation

(A) We presented tactile stimuli to four facial regions in awake mice: the whisker pad, the upper lip, the lower lip and the cheek. Each stimulus was delivered with a piezo-actuator that made a muted, yet audible sound which was also delivered without touch ("sound"). A blue light flash generated by an LED was used as visual stimulus. **(B)** To avoid interference of adjacent areas, we applied very gentle touches (0.686 mN). The complex spike response ratio was much reduced relative to the strong air puff stimulation to all ipsilateral whiskers illustrated in Figure 2. A fluorescent trace from a representative PC shows that responses to whisker pad stimulation could be evoked even with gentle stimulation. Sensory responses for all stimulus conditions in this cell are further illustrated by peri-stimulus time histograms (PSTHs) **(C)**. This particular PC responded to whisker pad, upper lip, lower lip and visual stimulation. Significance was calculated using a bootstrap method, with the black line representing the expected firing rate and the dashed line the average + 2 s.d. **(D)** For each stimulus condition, we averaged the PSTHs for all PCs that were responsive to that particular stimulus (colored lines; averages ± SEM). These were contrasted to the averaged PSTH of all non-responsive PCs (black lines; averages ± SEM). The pie charts represent the fraction of PCs responsive to each particular stimulus. **(E)** The peak responses were the lowest for sound and for upper lip stimulation. * $p < 0.05$; ** $p < 0.01$ (post-hoc tests after Kruskal-Wallis test) **(F)** As expected for complex spike responses to weak stimulation, the latencies were relatively long and variable, but consistent across types of stimulation. Only visual stimulation (LED) had a remarkably longer latency time. *** $p < 0.001$ (post-hoc tests after Kruskal-Wallis test for LED vs. whisker pad, upper lip, lower lip and cheek and $p < 0.05$ compared to sound)

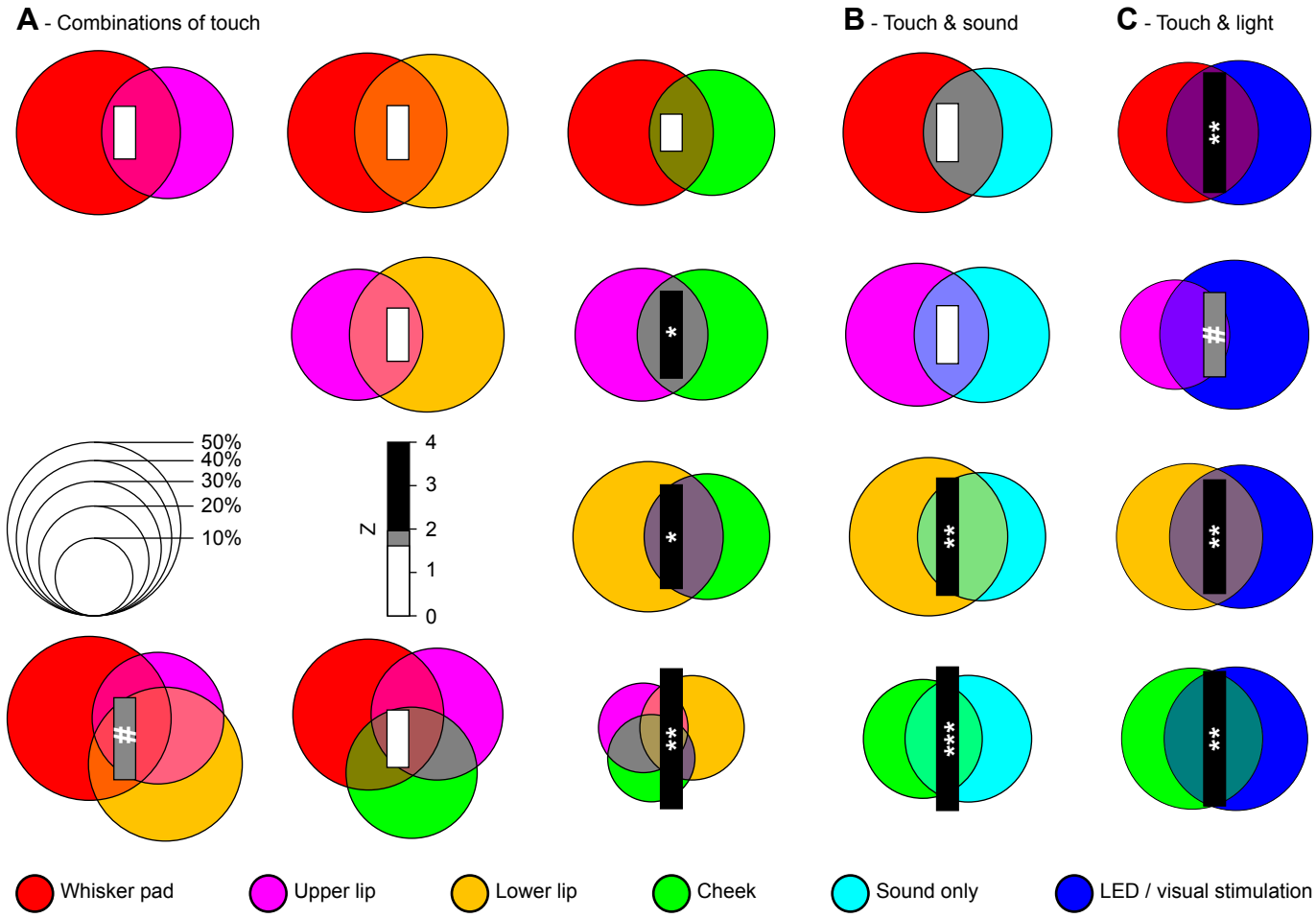

Figure 4 – Convergence of sensory input on PCs in crus 1 and crus 2

(A) PCs respond to multiple sources of sensory input (cf. Figure 3). We used a bootstrap method to evaluate whether PCs had a tendency towards segregating or integrating input from different sources. Venn diagram areas correspond to the fraction of PCs responsive to a particular stimulus. The rectangles are proportional to the *Z* score of the overlapping fraction (see scale bar). Grey bars denote a trend ($p < 0.10$) and black bars a significant convergence ($p < 0.05$). **(B)** Auditory and tactile stimuli had more overlap, as could be expected since tactile stimulation was always associated with the sound of the stimulator. The overlap was not complete, however, which might have been due to masking of the stimulator sound by high levels of ambient noise in the room. **(C)** Remarkably, visual and tactile input tended to converge, showing a preference of PCs for multi-modal input. # $p < 0.10$; * $p < 0.05$ and ** $p < 0.01$ after bootstrap analysis.

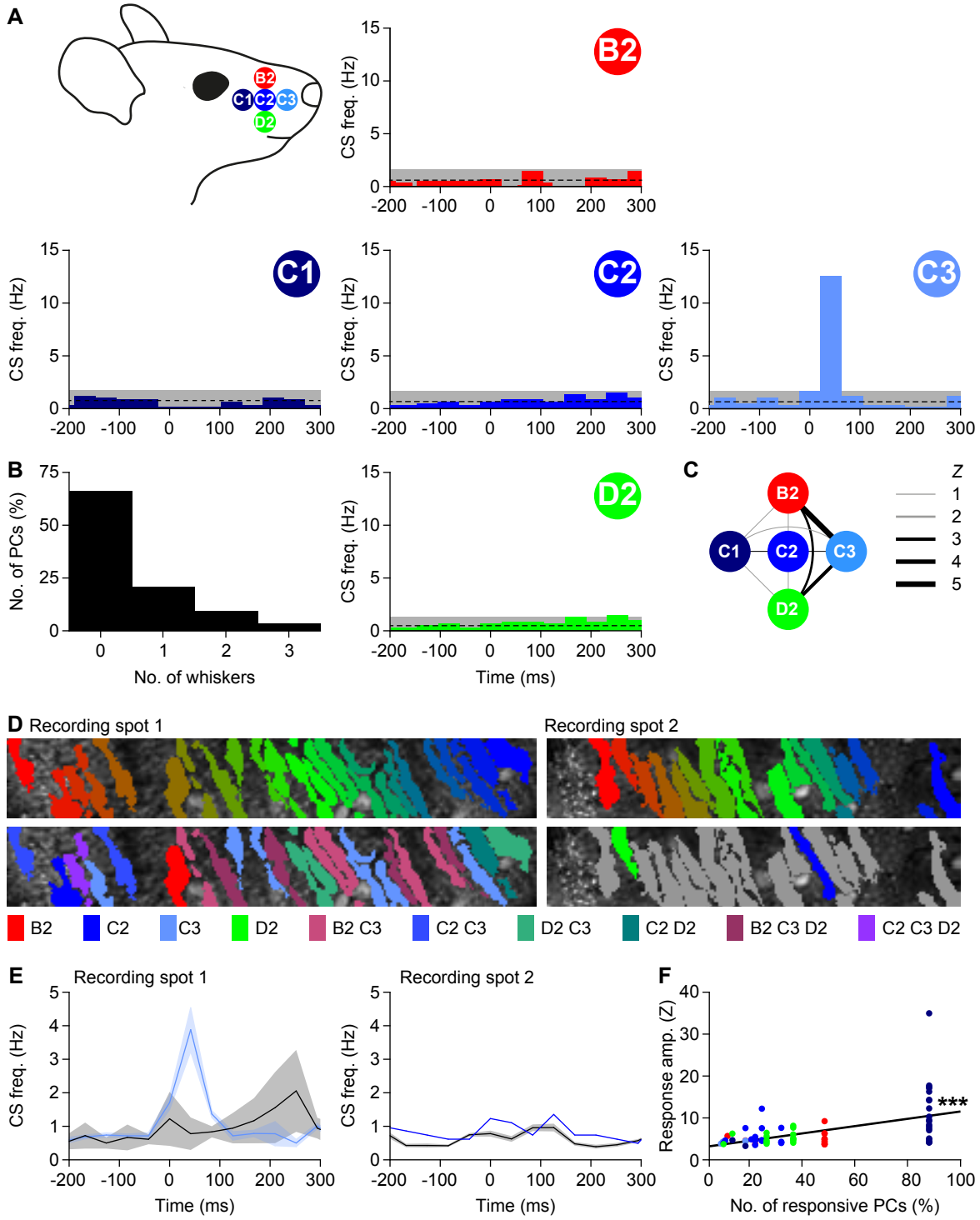

Figure 5 – PC responses to single whisker stimulation show weak clustering

(A) To investigate even smaller receptive fields, we stimulated sequentially five of the large facial whiskers. To avoid interference with other whiskers during active movement, we performed these experiments under ketamine/xylazine anesthesia. Most PCs, if responsive to single-whisker stimulation, responded only to one of the five whiskers **(B)**. This is illustrated by five peri-stimulus time histograms (PSTHs) from a single, representative PC. This particular PC was sensitive to stimulation of the C3 whisker only. The average and 3 s.d. of the baseline firing are indicated (dashed line and grey area). **(C)** PCs that responded to more than one whisker were typically responsive to the more anterior whiskers (see also Table 4). The widths of the lines indicate the *Z* value of the occurrence of multiple responses per cell. **(D)** Two recording spots, located close together in crus 1 of the same mouse, with the identified PC dendritic trees (pseudo-colored in *top row*). For each dendrite, the *bottom row* shows, in a different color coding scheme (see below the panels), the whisker(s) to which it was responsive (grey indicates no responses). **(E)** For each region, the average (± s.d.) of the responsive and the non-responsive PCs was indicated (to the C3 whisker in the left panel and to the C2 whisker in the right panel). Note that only a single cell was responsive in recording spot 2. The firing pattern of the non-responsive cells was also averaged (*black shades*). **(F)** Linear regression revealed that PCs that were surrounded by other PCs responsive to the same whisker (same color code as in **A**) had a tendency to show stronger responses to stimulation of that whisker than PCs that were more isolated. The *x*-axis represents the fraction of PCs responsive to the particular whisker within the respective field of view. R = 0.521; $p < 0.001$.

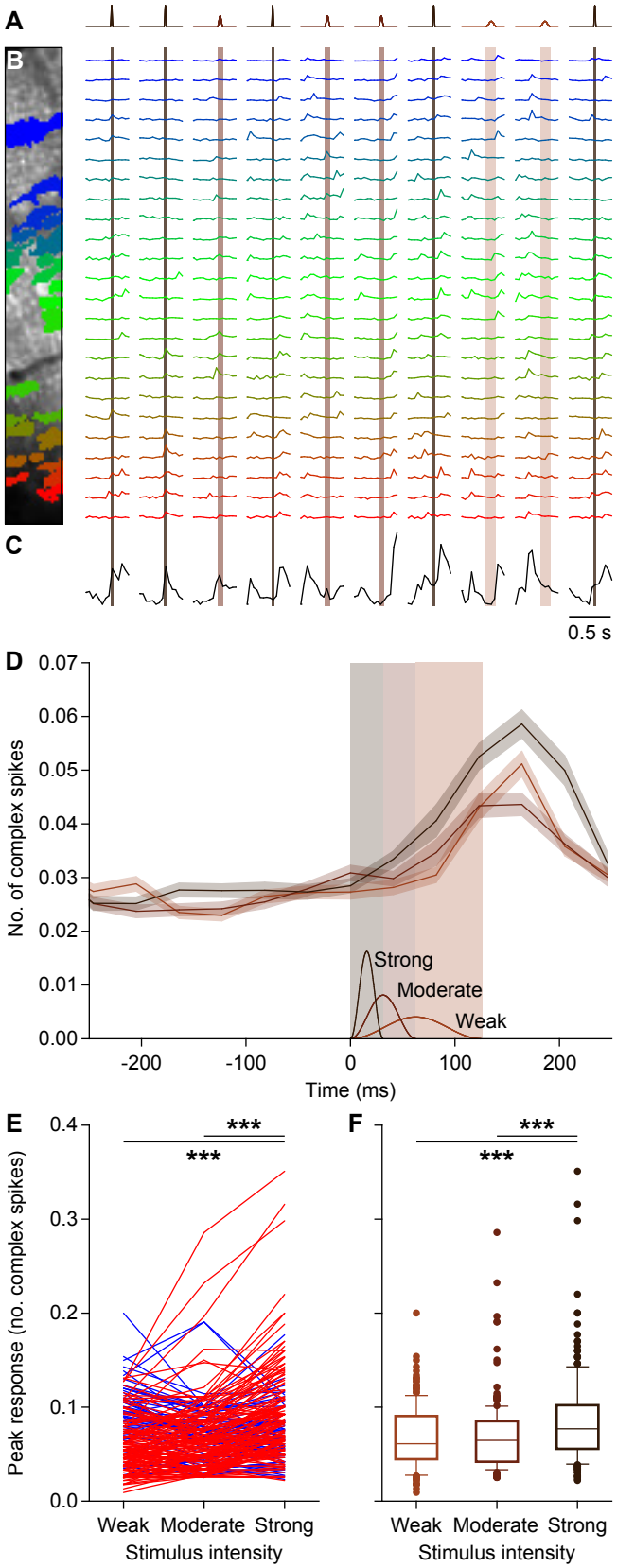

Figure 6 – Stimulus strength has only a minor impact on complex spike responsiveness

(A) Movements of all large facial whiskers were performed using a piezo-actuator at three different speeds (weak: 1 mm displacement in 62 ms; moderate: 2 mm displacement in 31 ms; strong: 4 mm displacement in 16 ms). The stimulus sequence was randomly permuted. **(B)** Field of view with 24 identified and color coded PCs (*left*) and their fluorescent traces (*right*). Stimuli were presented every 2 s and in between trials the laser illumination was briefly blocked to avoid photobleaching. The vertical shaded areas indicate the duration of the stimulus (which was inverse with the stimulus strength). **(C)** Summed fluorescence trace composed of all 24 individual traces showing that not all trials evoked ensemble-wide responses. **(D)** The average number of complex spikes per frame (of 40 ms) per trial (shaded areas: ± SEM) for the three stimulus strengths show little difference for the weak and moderate stimulation. The time course and amplitude (1-4 mm) of the three stimuli is schematized at the bottom of the graph. The strong stimulation elicits approx. 30% more complex spikes, as evident from the peak responses for each stimulus intensity **(E)**. The PCs that showed increased responsiveness to stronger stimuli are depicted in red and the others in blue. **(F)** The same data summarized with box plots for all responsive cells. Data are from 209 responsive PCs (out of 340 PCs that were measured in this way). *** $p < 0.001$ (Friedman's test).

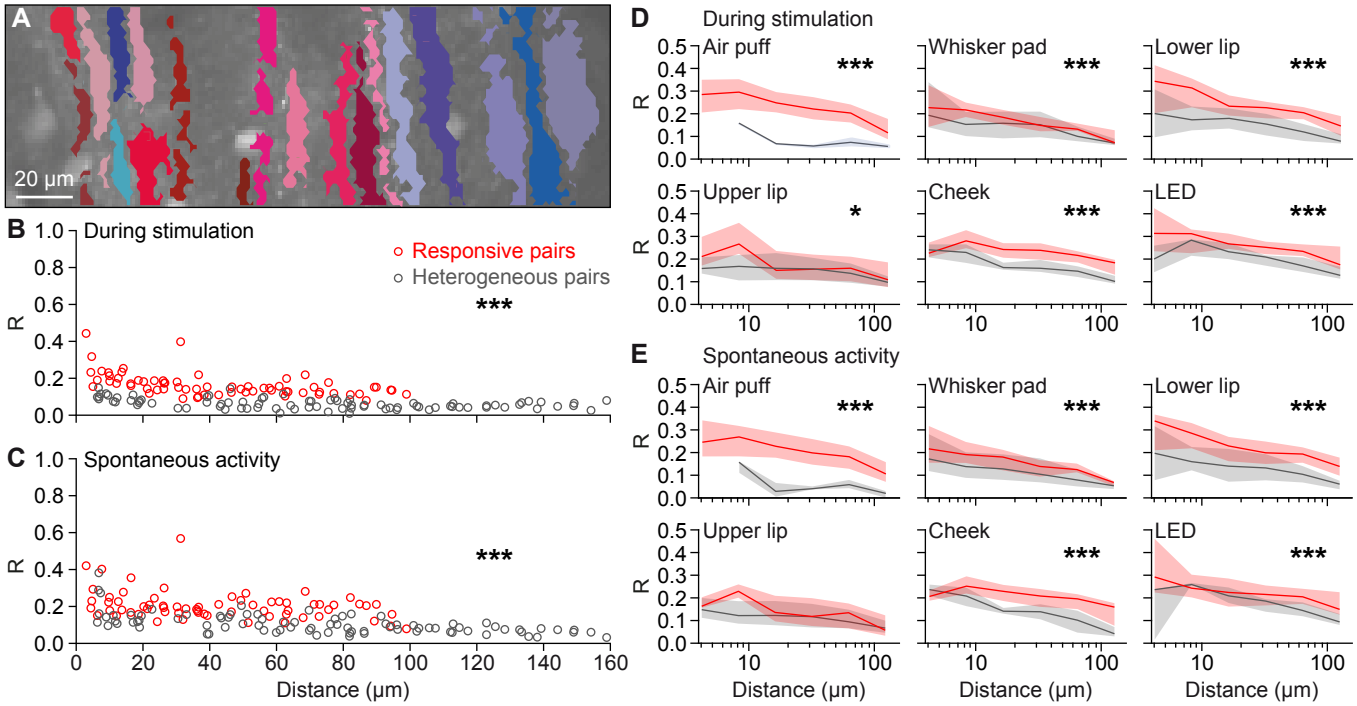

Figure 7 – PCs encoding the same response are closer together
(A) Representative field of view with segmented PC dendrites. Non-responsive cells are depicted in shades of blue and responsive cells in shades of red during whisker pad stimulation. **(B)** For each pair of PCs we calculated the correlation coefficient (R) during 1 Hz whisker pad stimulation. The pairs of two PCs that were both responsive to whisker pad stimulation had on average a higher level of coherence than the pairs connecting a responsive and a non-responsive PC ($p < 0.001$; two-dimensional Kolmogorov-Smirnov test). The pairs consisting of two non-responsive PCs were excluded from this analysis. **(C)** Interestingly, even in the absence of sensory stimulation, the pairs of PCs that were both responsive to whisker pad stimulation maintained a higher level of coherence than "heterogeneous pairs". Thus, PCs with the same receptive field tended to fire more coherently, even in the absence of stimulation. This analysis was expanded in the presence **(D)** and absence **(E)** of sensory stimulation for six different types of stimulation and illustrated as the median R value per distance category (six bin values of equal distance at a log scale). The shaded areas represent the inter-quartile ranges. * $p < 0.05$; *** $p < 0.001$ (Kolmogorov-Smirnov tests)

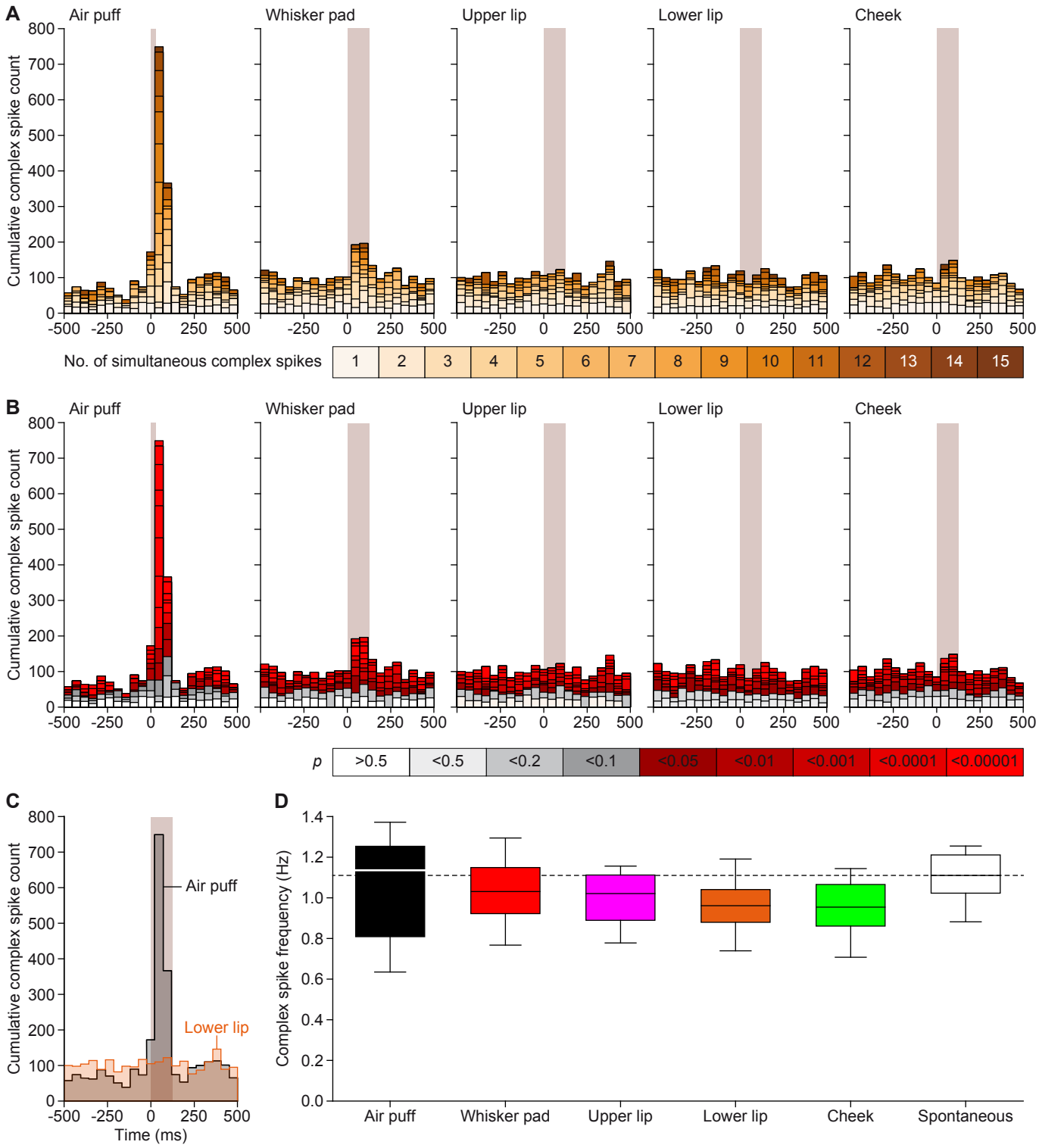

Figure 8 – PCs encode strong and weak sensory stimulation via synchronous firing

(A) Aggregate peri-stimulus time histograms (PSTHs) show that coherent firing of complex spikes predominantly occurs following sensory stimulation. For each field of view, we calculated the number of complex spikes occurring per frame. Subsequently, we made aggregate PSTHs where the color of each bin refers to the number of dendrites simultaneously active. In this field of view, 17 PCs were measured. Of these, 17 (100%) reacted to air puff, 12 (71%) to whisker pad, 3 (18%) to upper lip, 4 (24%) to lower lip and 1 (6%) to cheek stimulation. **(B)** Based upon a Poisson distribution of complex spikes over all dendrites and bins, one would expect between 0 and 3 simultaneously active dendrites (*grey bars*). The *red bars* indicate events involving more dendrites simultaneously than expected from a random distribution. Thus, the sparse firing as expected by chance is relatively constant throughout the trials, but the simultaneous activity of multiple dendrites is strongly enhanced following sensory stimulation. **(C)** A direct overlay of the aggregate PSTHs in response to air puff and lower lip stimulation shows that the strong response found after air puff stimulation comes at the expense of inter-trial complex spikes (152 trials per condition). **(D)** For equally long recordings in the presence of different types of stimulation, equal complex spike frequencies were observed as during spontaneous activity ($F(2.544, 20.348) = 2.561$, $p = 0.091$, repeated measures ANOVA), indicating that sensory stimulation results in a temporal re-ordering of complex spikes, rather than to the production of more complex spikes.

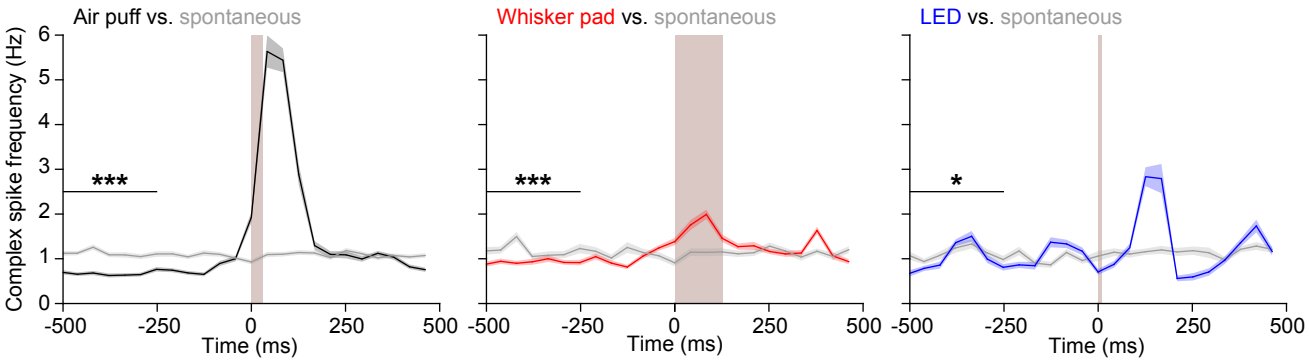

Figure 9 – Sensory stimulation results in a temporal re-ordering of complex spikes
The temporal distribution of complex spikes was compared between periods with sensory stimulation and periods without. For this analysis, we included only PCs that displayed a significant response to the stimulus involved (n = 117 for air puff, n = 45 for whisker pad and n = 27 for visual stimulation). Irrespective of the type of stimulation, a reduction in inter-trial activity was found. This was quantified by during the period between 500 and 250 ms prior to stimulus onset using paired t tests; * and *** indicate $p < 0.05$ and $p < 0.001$, respectively.